ANALYSIS OF A LOW ENRICHED URANIUM CENTRIFUGAL GAS CORE REACTOR

by

Darrin Leer

A thesis submitted to the faculty of
The University of North Carolina at Charlotte
in partial fulfillment of the requirements
for the degree of Master of Science in
Applied Physics

Charlotte

2020

Approved by:

____

Dr. Donald Jacobs

____

Dr. Susan Trammell

____

Dr. Russell Keanini

ABSTRACT

DARRIN LEER. Analysis of a Low Enriched Uranium Centrifugal Gas Core Reactor. (Under the direction of DR. DONALD JACOBS)

With the new NASA directive of returning to the Moon in 2024 as a stepping stone to missions to Mars and beyond, there is a renewed interest in developing nuclear thermal rockets (NTR) to reduce trip times. This thesis will focus on the analysis of a conceptual reactor design for use as an NTR. The low enriched uranium centrifugal gas core reactor (CGCR) is a low technology readiness level (TRL) concept that uses centrifuge technology to separate uranium gas from hydrogen propellant. There is also a new US directive for additional focus on research and development of reactors that utilize low enriched uranium (LEU) instead of high enriched uranium (HEU). The inclusion of a moderator in between the gas enables the use of LEU and a lower mass system compared to previous gas core concepts. In addition, the CGCR operates at lower temperatures than previous gas core concepts enabling higher uranium densities, which suggests that the centrifugal separation will aid in minimization of uranium entrainment. This research will cover a thorough analysis of neutronics, thermal transport, fluid dynamics, and comparison to alternative NTR designs utilizing computational methods, such as the Monte Carlo N-Particle transport code MCNP, and analysis software platforms Mathematica and MATLAB.

ACKNOWLEDGEMENTS

I'd like to acknowledge Dr. Michael Houts from NASA for acting as nuclear thermal propulsion subject matter expert, Dr. Russell Keanini for insight and assistance in developing the fluid dynamics model for this research, Dr. Susan Trammell for acting as committee member, and Dr. Donald Jacobs as my primary advisor.

TABLE OF CONTENTS

LIST OF FIGURES

LIST OF ABBREVIATIONS

CGCR	Centrifugal Gas Core Reactor
GCR	Gas Core Reactor
HEU	High Enriched Uranium
LEU	Low Enriched Uranium
MCNP	Monte-Carlo N-Particle
NASA	National Aeronautics and Space Administration
NTP	Nuclear Thermal Propulsion
NTR	Nuclear Thermal Rocket
PBR	Particle Bed Reactor
SNTP	US Space Nuclear Thermal Propulsion
TRL	Technology Readiness Level
US	United States

CHAPTER 1: INTRODUCTION

1.1 Motivation

Long-term human space exploration missions come with many challenges and an increasing level of risk. One way to reduce that risk to make missions beyond the moon more feasible is to make the journey less long term. The best way to do that is to make our rockets faster by making advancements in propulsion technologies. With the new NASA directive of returning to the Moon in 2024 as a stepping stone to missions to Mars and beyond, there is a renewed interest in developing nuclear thermal rockets (NTR) to reduce trip times. This thesis will focus on the analysis of a conceptual reactor design for use as an NTR. The low enriched uranium centrifugal gas core reactor (CGCR) is a low technology readiness level (TRL) concept that uses centrifuge technology to separate uranium gas from hydrogen propellant. There is also a new US directive for additional focus on research and development of reactors that utilize low enriched uranium (LEU) of enrichment less than 20% instead of high enriched uranium (HEU). Some NASA studies suggest that in order to accomplish a round-trip mission to Mars, a high thrust engine with a specific impulse, I_{sp}, greater than 1300 seconds may be required.[4][5] Specific impulse is defined as the total impulse delivered per unit of propellant consumed, and is equivalent to the generated thrust divided by the mass flow rate.

Modern chemical rockets have high thrust, but still require an enormous amount of fuel, having an $I_{sp} \sim 500$s, making them less efficient for longer journeys. Nuclear thermal propulsion (NTP) is an alternative to chemical rockets that provide a boost to the I_{sp} numbers. Current NTP designs estimate I_{sp} double the most advanced chemical rockets at comparable thrust values. In addition to the resulting faster transit times, NTP engines could double as or be converted for electric power generation, as well as being expected to double or triple payload capacity compared to chemical propellants.

First generation NTP engines are limited to an $I_{sp} \sim 900$s, with designs for up to ~ 2000s. However, no significant work has been performed since the 1970s, due to changes in NASA policies and the spectre that comes with the words "nuclear" and "rocket". With this renewed initiative to continue work on NTP systems, new generation concepts are needed; particularly, ones that build on 1st Generation designs and experience.

One approach is to build on designs used in the US Space Nuclear Thermal Propulsion (SNTP) program. These designs used relatively large nuclear fuel elements in a moderator block where propellant would flow through the fuel elements. Nuclear fuel in the SNTP engine design was held in place using a "cold frit" and a "hot frit" to allow hydrogen to flow radially inward through the fuel and then exit axially at high temperature.[4] This can be seen in Figures 1.1 & 1.2.

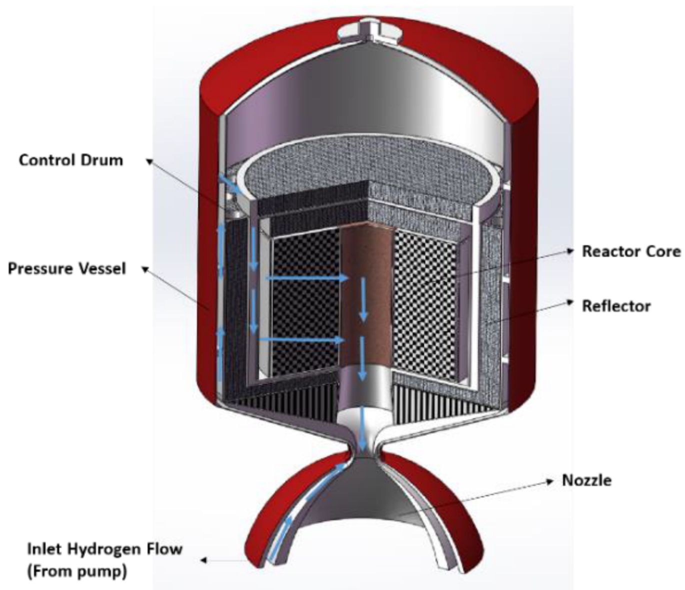

(a)

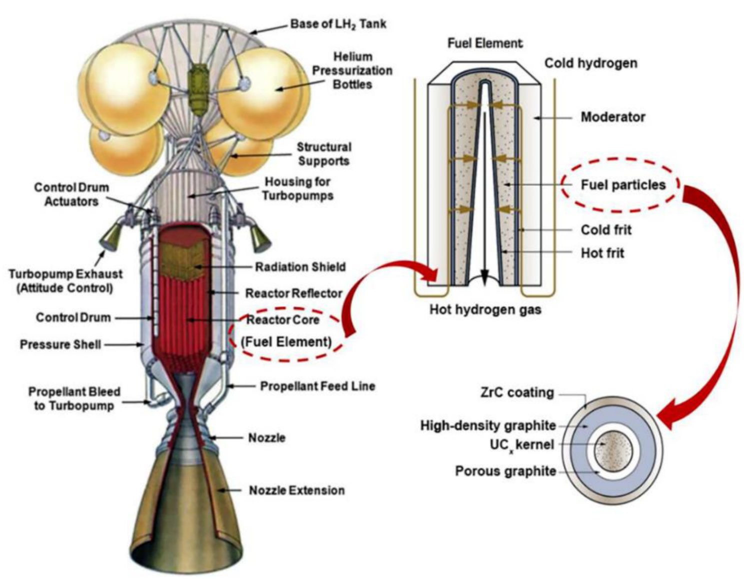

(b)

Figure 1.1: Schematic view of a particle bed reactor (PBR) for propulsion. (a) Individual PBR core; (b) fuel elements-assembled PBR core [1]

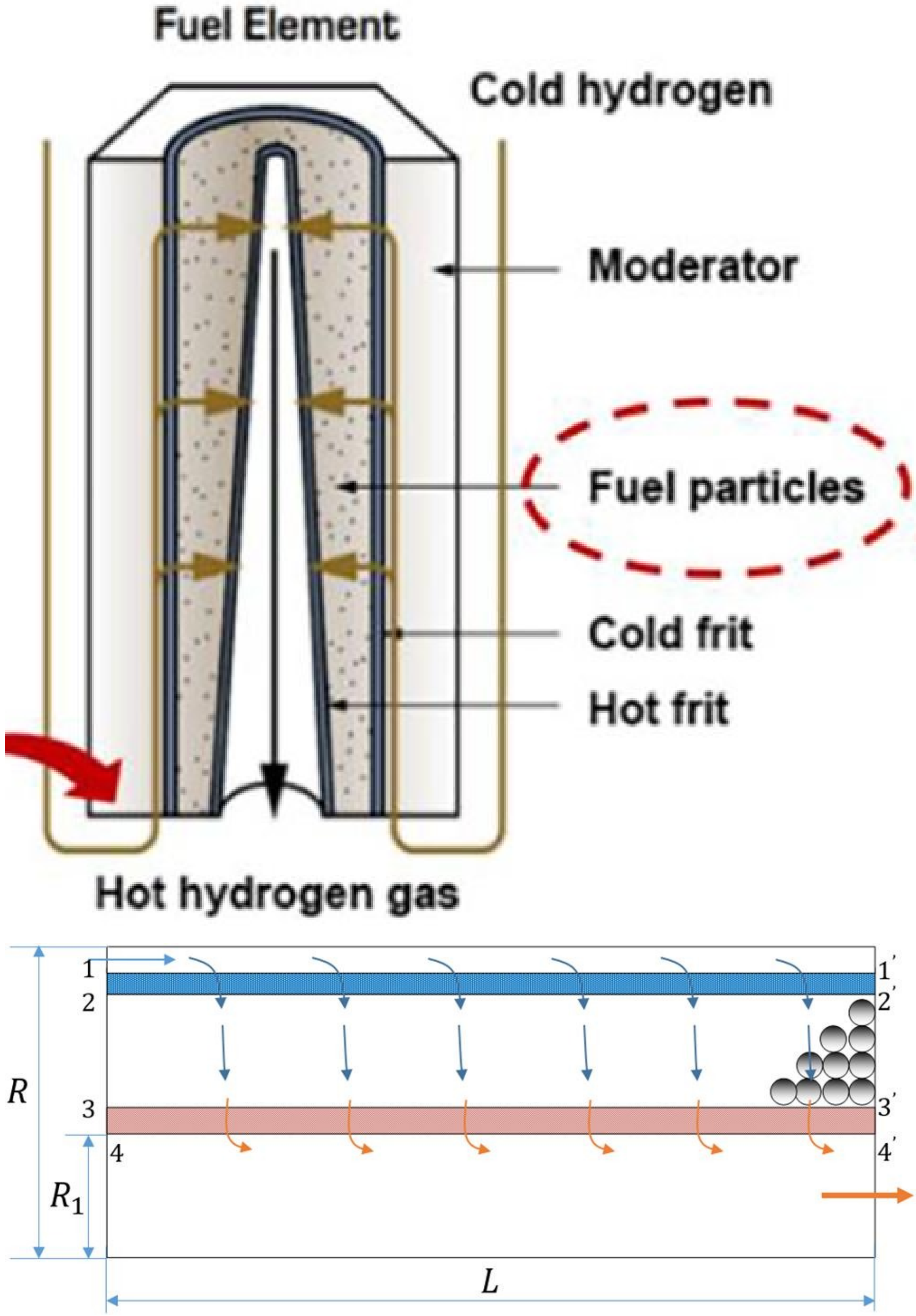

Figure 1.2: Schematic view of a particle bed reactor (PBR) fuel element and its simplification [1]

A similar concept for a 2nd Generation NTP system would utilize centrifugal force as a means of fuel containment instead of the "hot frit" element, allowing for portions of the fuel to operate beyond its melting point. This centrifuge concept could yield good separation between propellant and nuclear fuel. This particular design is the focus of this research and can be seen in Figures 1.3 & A.1.

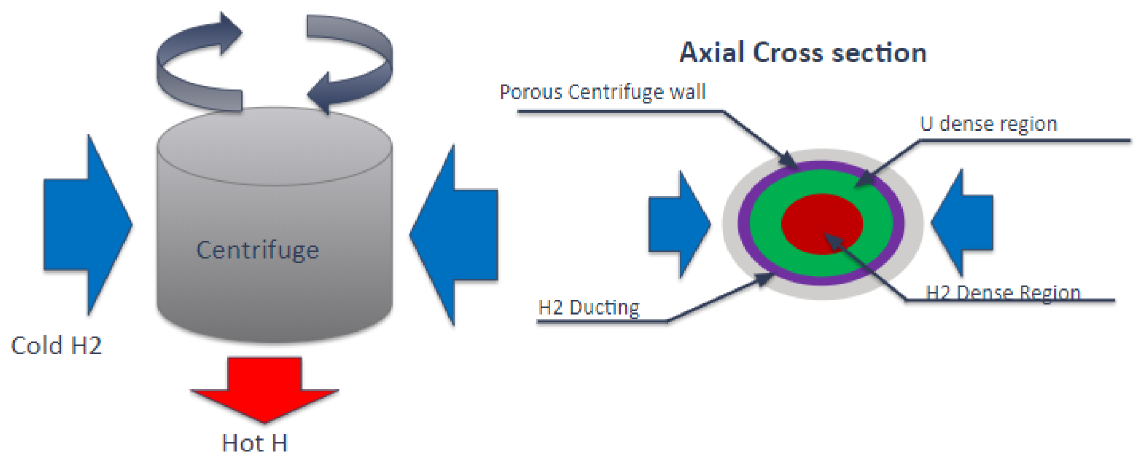

Figure 1.3: Rotating radial in-flow fuel element (no hot frit)[2]

The centrifugal gas core reactor can be explored in theory by initially looking at a model of the heat transfer, growth, and dynamics of radially-injected hydrogen bubbles in a rotating finite multi-phase fluid system under zero-gravity. As the CGCR is a nuclear reactor, it is necessary to determine its criticality, and having a proper density profile of nuclear fuel is highly important in this determination. This problem is coupled in nature: the density profile as a function of temperature, which is a function of nuclear heating, which is determined by the density profile of the nuclear fuel. Therefore, an iterative approach must be employed initially to determine the proper density profile.

1.2 Problem Statement

The design of this reactor fuel element, as seen in Figures 1.4 & 1.5, consists of coaxial annular cylinders of uranium metal housed by a porous cold frit (graphite), hydrogen coolant region, and a reflector/moderator/pressure vessel material, with a central hot hydrogen plenum. Rotating elements are rotating with angular velocity Ω. Cold hydrogen will flow radially inward through the cold frit, through the uranium fuel layer, and then finally exiting axially at high temperature.

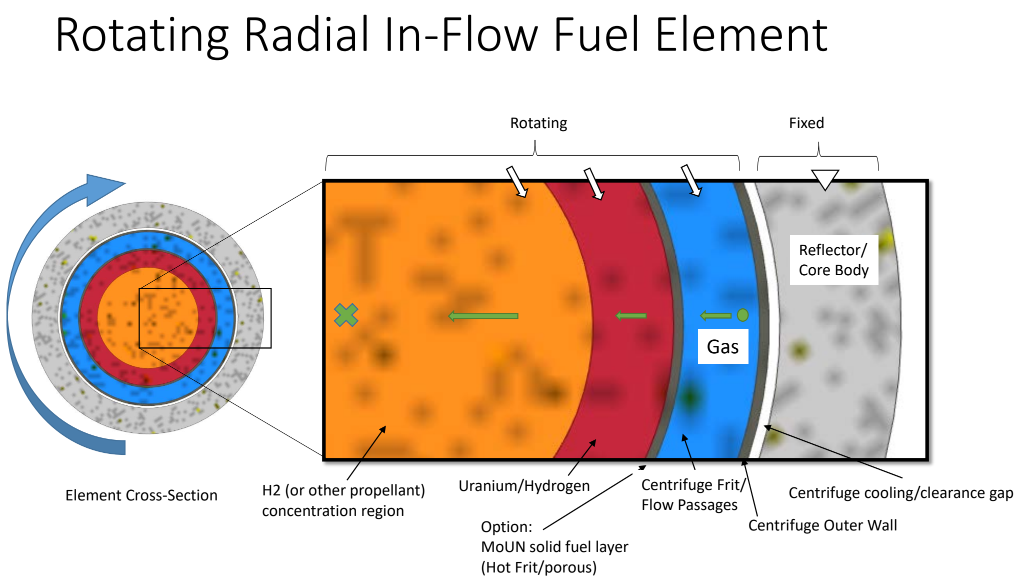

Figure 1.4: Rotating radial in-flow fuel element (no hot frit)[2]

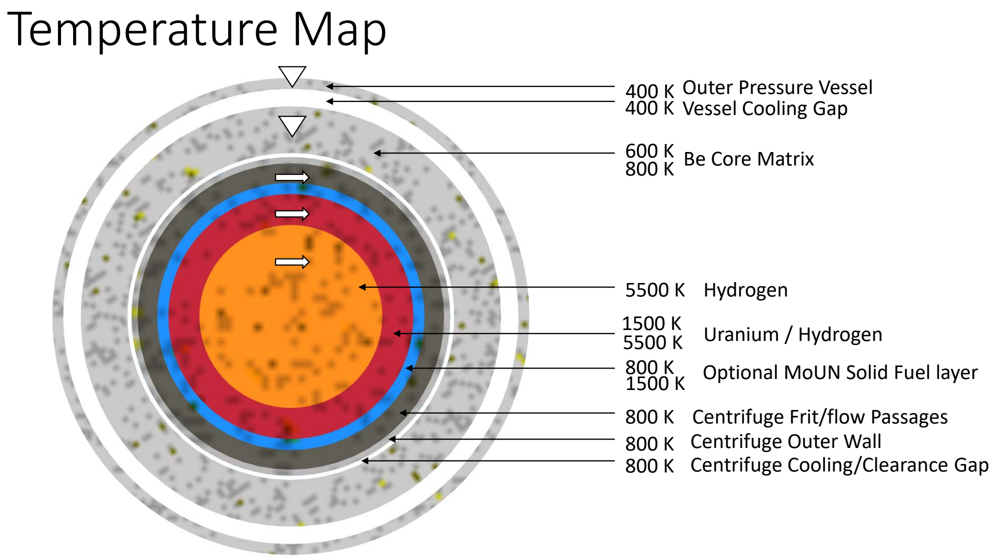

Figure 1.5: Temperature map of rotating radial in-flow fuel element (no hot frit)[2]

In this model, Figure 1.6, a hydrogen bubble is traveling radially inward through a layer of high density multi-phase fissioning uranium metal, passing into a central hydrogen plenum. The reactor is designed with a Beryllium pressure vessel of $OD = 100cm$ and length 110cm, a Li_7H reflector of thickness 1cm and $OD = 14.2cm$, a hydrogen coolant region of thickness 1mm and $OD = 12.2cm$, a porous graphite frit with H_2 ducting of thickness 1cm and $OD = 12cm$, LEU uranium region (19.75% enrichment) with $OD = 10cm$, hot dense hydrogen region $OD = 6cm$; the non-Beryllium region is 100cm in length. Where r_u is the outer radius of the uranium layer, r_{u_f} is the location of the interface between solid and liquid uranium, r_{u_v} is the location of the interface between liquid and vapor uranium, and r_p is the location of the interface between uranium and the hot hydrogen plenum.

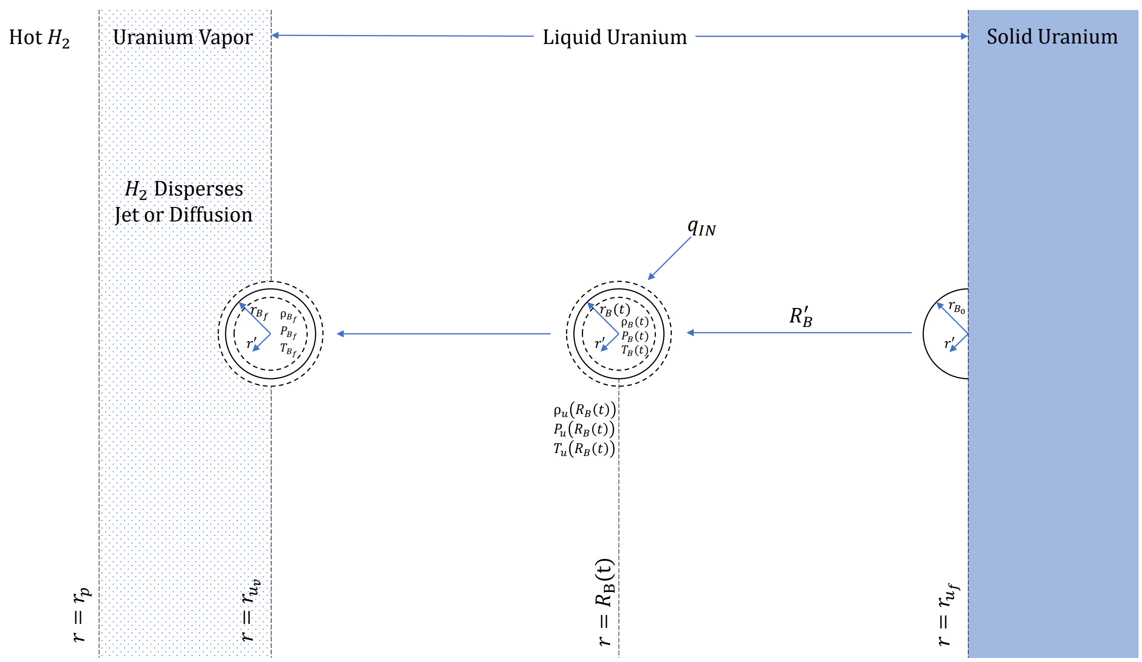

Figure 1.6: Hydrogen bubble traveling through uranium layer

CHAPTER 2: MODEL: Theory and Methods

This chapter will demonstrate the building of a model framework that describes several coupled equations that will be solved numerically for a single hydrogen bubble traveling through the liquid uranium layer. In reality there will be more than one bubble traveling the same streamline through the uranium layer, as new bubbles will be formed as each bubble travels radially inward away from the site of injection; however, until a basic model of a single bubble is determined, bubble-bubble interactions will not be discussed. A more accurate model, for the purposes and use as an NTR, may in fact be a column or jet of hydrogen, but as an initial model, a single spherical bubble will be discussed. For this initial model, it is assumed that once the bubble reaches the uranium vapor, the bubble will disperse and become well-mixed within the uranium vapor. Molecular Hydrogen (H_2) is considered, however dissociation may need to be explored in later models. To take advantage of the rotational symmetry of the cylindrical reactor, this model will be built in a cylindrical coordinate system. The desired model seeks to simultaneously calculate the uranium layer temperature, density, and pressure profiles; the bubble temperature, position, and radius; as well as solve for the nuclear fission effective multiplication factor, and the energy deposition rate. The variables will be defined as $T_u(r)$, $\rho_u(r)$, $P_u(r)$, $T_B(t)$, $R_B(t)$, $r_B(t)$, k_{eff}, and E_d, respectively. Fluid dynamics, heat transfer, and neutronics must be explored in order to determine the performance of this reactor concept.

2.1 Bubble Energy Balance

A good starting point for this model will begin by developing a governing equation that includes many of the above unknowns. Starting from the energy balance on the bubble, we have:

a) $dt \int_{V_B(t)} \rho_B c_{p_B} T_B dV = \oint_{S_B(t)} \mathbf{q} \cdot \hat{n} dA$

b) $c_{p_B} \frac{d}{dt}(\rho_B T_B) V_B = q_{IN}(t) 4\pi r_B^2(t) + \frac{dP_B}{dt} V_B$

Given that $q_{IN} = h[T_u(R_B(t)) - T_B(t)]$

$$c_{p_B} \frac{d}{dt}(\rho_B T_B) V_B = h[T_u(R_B(t)) - T_B(t)] 4\pi r_B^2(t) + \frac{dP_B}{dt} V_B \tag{2.1}$$

where $h, c_{p_B}, \rho_B, R_B, r_B, T_B, T_u(R_B(t))$ are the convective heat transfer coefficient, specific heat of the bubble, bubble density, bubble position relative to plenum centerline, bubble radius, bubble temperature, and uranium temperature at $R_B(t)$, respectively, and the bubble volume is $V_B(t) = \frac{4}{3}\pi r_B^2(t)$ and the bubble surface area is $S_B(t) = 4\pi r_B^2(t)$. Equation (2.1) assumes that the hydrogen is well-mixed at all times (t) within the bubble, the uranium temperature (T_u) is uniform around bubble, and the bubble is spherical.

Assuming H_2 behaves as a real gas:

$$\rho_B(t) = \frac{P_B(t)}{Z R_{H_2} T_B(t)} \tag{2.2}$$

$$R_{H_2} = \frac{\bar{R}}{MW_{H_2}} \tag{2.3}$$

where R_{H_2} is the specific gas constant of hydrogen, $\bar{R}$ is the ideal gas constant, and Z is the compressibility factor of hydrogen.

If we take $t = 0$ to be the instant that the bubble is injected into the uranium layer, then the initial conditions can be set as $P_B(t = 0) = P_0$, $T_B(t = 0) = T_0$, $\rho_B(t = 0) = \frac{P_0}{Z R_{H_2} T_0}$, $r_B(t) = r_{B0}$, and $R_B(t = 0) = r_{u_f}$, where r_{u_f} is the location of the interface between solid and liquid uranium. We now have multiple time-dependent unknowns: $T_B(t)$, $P_B(t)$, $T_u(R_B(t))$, $R_B(t)$, and $r_B(t)$.

In order to tackle the above unknowns, we can start with the Young-Laplace equation:

$$P_B(t) - P_u(R_B(t)) = \frac{2\sigma_{st}}{r_B(t)} \tag{2.4}$$

where $P_u(R_B(t))$ is the pressure in the uranium layer at $R_B(t)$, and σ_{st} is the surface tension coefficient for the uranium-hydrogen interface. At the melting point, the surface tension is approximately 1500 dynes/cm according to [6] and [7].

Equation (2.4) introduces a new unknown $P_u(r)$, which we can assume $P_u(r)$ is calculable via the Navier-Stokes equations applied within the uranium layer, allowing us to determine $r_B(t)$.

2.2 U-Layer Heat Transfer

In order to find for temperature distribution $T_u(r)$, which is assumed to be steady-state, we will need to use the energy equation [8][9] applied within the uranium layer:

$$\rho_u c_{p_u} \left[\frac{u_\theta T_{u,\theta}}{r} + u_r T_{u,r} \right] = K_u \left[T_{u,rr} + \frac{T_{u,r}}{r} \right] + \dot{S}(r) \tag{2.5}$$

where ρ_u, c_{p_u}, K_u are the density, specific heat, and thermal conductivity of uranium, respectively; $\dot{S}(r)$ is the volumetric heating term due to nuclear heating; $u_\theta = u_\theta(r)$ is the θ-velocity component in the uranium layer; u_r is the r-velocity component in the uranium layer, which we assume is negligible, and therefore:

$$u_r = 0 \tag{2.6}$$

If we assume the fluid cylinder has rotational symmetry, then T_u is symmetric:

$$\Rightarrow T_{u,\theta} = 0 \tag{2.7}$$

Equation (2.5) assumes K_u is fixed across u-layer, however since ΔT_u is large, it may be worth exploring a variable K_u in further study via $\Phi_q = -K\nabla T$. In this model, we will also neglect axial variation in T_u. Using the above assumptions, equation (2.5) reduces to:

$$\frac{d^2T_u}{dr^2} + \frac{1}{r}\frac{dT_u}{dr} + \frac{\dot{S}(r)}{K_u} = 0 \tag{2.8}$$

For any given $\dot{S}(r)$, (2.8) can be solved numerically, or analytically, if $\frac{d\dot{S}(r)}{dr} << 1$, by further assuming $\dot{S}(r) \approx \text{constant} \equiv \dot{S}_0$. Then (2.8) becomes:

$$T_u'' + \frac{1}{r}T_u'' + \frac{\dot{S}_0}{K_u} = 0 \tag{2.9}$$

2.3 U-Layer Fluid Dynamics

In order to determine $r_B(t)$ in equation (2.4) we first need to find the pressure distribution in the U-Layer, $P_u(r)$.

a) Working in cylindrical coordinates, the Navier-Stokes equation for the azimuthal component θ [9]:

$$\rho_u\left[u_r u_{\theta,r} + u_z u_{\theta,z} + \frac{u_\theta}{r}u_{\theta,\theta} + \frac{u_r u_\theta}{r}\right] = -\frac{1}{r}\frac{\partial P_u}{\partial \theta} + \mu_u\left[u_{\theta,rr} + \frac{u_{\theta,r}}{r} - \frac{u_\theta}{r^2}\right]$$

Assuming u_z is negligible, $u_{,rr} = u_{,zz} = 0$, symmetry of the velocity field, neglecting temperature-dependence of μ_u(uranium viscosity), neglecting presence of hydrogen bubbles, and taking into account equation (2.6), the above equation reduces to:

$$\Rightarrow \frac{1}{r}\frac{d}{dr}\left(r\frac{du_\theta}{dr}\right) - \frac{u_\theta}{r^2} = 0 \tag{2.10}$$

Solving (2.10) analytically gives:

$$u_\theta(r) = r\Omega_0 \tag{2.11}$$

where Ω_0 is the angular velocity of the cylinder.

b) From the r-component of the Navier-Stokes equation:

$$-\rho_u \frac{u_\theta^2}{r} = -\frac{\partial P_u}{\partial r} \tag{2.12}$$

and since P_u = function of r only:

$$\Rightarrow \frac{\partial P_u}{\partial r} = \frac{dP_u}{dr} \tag{2.13}$$

As the u-layer consists of solid, liquid, and gas, densities of each region will be different:

$$\rho_u(r) = \begin{cases} \rho_{u_s}(r) = Constant & r_{u_f} \leq r \leq r_u \\ \rho_{u_l}(r) = 17270 - 1.4485(T_u(r) - 1408) & r_{u_v} \leq r < r_{u_f} \\ \rho_{u_v}(r) = \frac{P_u(r)}{R_u T_u(r)} & r_p \leq r < r_{u_v} \end{cases} \tag{2.14}$$

where R_u is the specific gas constant for uranium, and the density for liquid uranium comes from [10][11].

Using (2.11), (2.13), and the vapor region of (2.14), we can rearrange (2.12) in terms of $\rho_{u_v}(r)$:

$$\rho_{u_v}(r) r \Omega_0^2 = \frac{d}{dr}(\rho_{u_v}(r) R_u T_u(r))$$

Solving for $\rho_{u_v}(r)$ gives:

$$\rho_{u_v}(r) = C \exp\left[\frac{\Omega_0^2 r^2}{2R_u T_u(r)}\right], \qquad r_p \leq r < r_{u_v} \tag{2.15}$$

Given the B.C.s of:

$$P_{u_v}(r_{u_v}) = P_{u_l}(r_{u_v})$$

$$\rho_{u_v}(r_{u_v}) = \frac{P_{u_v}(r_{u_v})}{R_u T_u(r_{u_v})}$$

we can solve for the constant in (2.15), giving:

$$\rho_{u_v}(r) = \frac{P_{u_l}(r_{u_v})}{R_u T_u(r_{u_v})} \exp\left[\frac{\Omega_0^2}{2R_u}\left[\frac{r^2}{T_u(r)} - \frac{r_{u_v}^2}{T_u(r_{u_v})}\right]\right], \qquad r_p \le r < r_{u_v} \tag{2.16}$$

Plugging (2.16) back into (2.14) and using (2.12) to solve for $P_u(r)$, we find:

$$\rho_u(r) = \begin{cases} Constant & r_{u_f} \le r \le r_u \\ 17270 - 1.4485(T_u(r) - 1408) & r_{u_v} \le r < r_{u_f} \\ \frac{P_u(r_{u_v})}{R_u T_u(r_{u_v})} \exp\left[\frac{\Omega_0^2}{2R_u}\left[\frac{r^2}{T_u(r)} - \frac{r_{u_v}^2}{T_u(r_{u_v})}\right]\right] & r_p \le r < r_{u_v} \end{cases} \tag{2.17}$$

$$P_u(r) = \begin{cases} Constant & r_{u_f} \le r \le r_u \\ \int \rho_u(r) r \Omega_0^2 dr & r_{u_v} \le r < r_{u_f} \\ \rho_u(r) R_u T_u(r) & r_p \le r < r_{u_v} \end{cases} \tag{2.18}$$

This analysis of rotating immiscible gases can generalize the above density and pressure functions to:

$$\rho_j(r, \Omega) = C_j \exp[\Omega^2 r^2 / 2R_j T_j(r)] \tag{2.19}$$

$$P_j(r, \Omega) = \rho_j(r, \Omega) R_j T_j(r) \tag{2.20}$$

where j represents differing gas regions as seen in Figure 2.1.

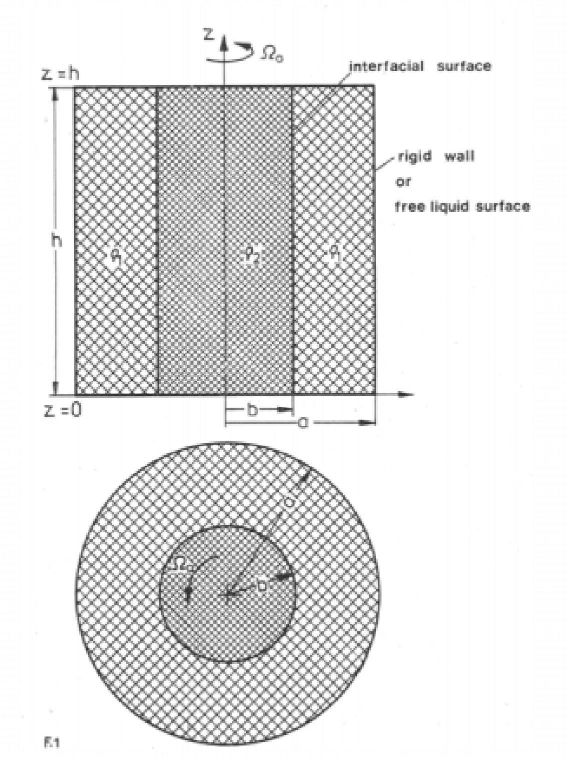

Figure 2.1: Rotating immiscible fluids [3]

When looking at the interaction between the gaseous uranium and the hydrogen plenum at the interface $r = r_p$,

$$P_u(r_p) = P_{H_2}(r_p)$$

And thus equation (2.19) for each gas yields:

$$\rho_{u_v}(r, \Omega_0) = \rho_u(r_p) \exp\left[\frac{\Omega_0^2}{2R_u T_u(r_p)}(r^2 - r_p^2)\right], \qquad r_p \leq r < r_{u_v} \tag{2.21}$$

$$\rho_{H_2}(r, \Omega_0) = \frac{P_u(r_p)}{R_{H_2} T_{H_2}(r_p)} \exp\left[\frac{\Omega_0^2}{2R_{H_2} T_{H_2}(r_p)}(r^2 - r_p^2)\right], \qquad 0 \leq r \leq r_p \tag{2.22}$$

Given the acceleration potentials for each region from Bauer [3], which consist of pressure and centrifugal terms:

$$\Psi_u = \frac{P_u - P_0}{\rho_u} - \frac{1}{2}\Omega_0^2(r^2 - r_p^2) - \frac{1}{2}\Omega_0^2\frac{\rho_{H_2}}{\rho_u}r_2^2 \tag{2.23}$$

$$\Psi_{H_2} = \frac{P_{H_2} - P_0}{\rho_{H_2}} - \frac{1}{2}\Omega_0^2 r^2 \tag{2.24}$$

At the interfacial surface $r = r_p$, the normal velocities of the U and H_2 regions are equal, and therefore the free surface boundary condition is given by:

$u_u = u_{H_2}$ at the interface $r = r_p$

$$\begin{aligned}\rho_{H_2}(r_p)\frac{\partial \Psi_{H_2}}{\partial t} - \rho_u(r_p)\frac{\partial \Psi_u}{\partial t} + (\rho_{H_2}(r_p) - \rho_u(r_p))r_p\Omega_0^2 u_{H_2} \\ + \frac{\sigma_{st_p}}{r_p^2}\left(u_{H_2} + \frac{\partial^2 u_{H_2}}{\partial \theta^2} + r_p^2\frac{\partial^2 u_{H_2}}{\partial z^2}\right) = 0\end{aligned} \tag{2.25}$$

where σ_{st_p} is the interfacial tension at $r = r_p$ between gases U and H_2 . If we assume steady state and that $u_{H_{2,zz}} = u_{H_{2,\theta\theta}} = 0$, then solving for r_p yields:

$$r_p = \left[\frac{\sigma_{st_p}}{\Omega_0^2\rho_u(r_p)\left(1 - \frac{\rho_{H_2}(r_p)}{\rho_u(r_p)}\right)}\right]^{\frac{1}{3}} \tag{2.26}$$

$\frac{\rho_{H_2}}{\rho_u} << 1$

$$r_p = \left[\frac{\sigma_{st_p}}{\Omega_0^2\rho_u(r_p)}\right]^{\frac{1}{3}} \tag{2.27}$$

This can also be stated in terms of the rotational Bond number $\widetilde{B}_0$:

$$\widetilde{B}_0 = \Omega_0^2 r_{u_v}^3 \rho_u(r_p)/\sigma_{st_p}$$

$$r_p = \frac{r_{u_v}^3}{\widetilde{B}_0} \tag{2.28}$$

2.4 Bubble Dynamics

Due to the pressure gradient within the uranium layer, a bubble injected radially inward will see a buoyant force, pushing the bubble inward from $r = r_{u_f}$ to $r = r_{u_v}$. Given $P_u(r)$, we can calculate the instantaneous radial pressure force, $F_{B_P}(t)$.

$$\begin{aligned}
F_{B_P}(t) &= -\oint_{S_B(t)} P_u \hat{n} \cdot \hat{e_r} dA \\
&= -\int_{V_B(t)} \nabla \cdot (P_u(r)\hat{e_r}) dV \\
&= -\int_{V_B(t)} \left[\hat{e_r}\frac{\partial}{\partial r} + \frac{\hat{e_\theta}}{r}\frac{\partial}{\partial \theta} \right] \cdot (P_u(r)\hat{e_r}) 4\pi r^2 dr \\
&= -\int_0^{r_B(t)} \left[\frac{dP_u(r)}{dr} + \frac{P_u(r)}{r} \right] 4\pi r^2 dr
\end{aligned}$$

As $P_u(r)$ will be evaluated over $r = R_B(t) + r'$:

$$F_{B_P}(t) = -\int_0^{r_B(t)} \left[\frac{dP_u(r)}{dr}|_{r=R_B(t)+r'} + \frac{P_u(r)|_{r=R_B(t)+r'}}{R_B(t) + r'} \right] 4\pi {r'}^2 dr' \tag{2.29}$$

The bubble is also subject to a drag force $F_{B_D}(t)$ and a centrifugal force $F_{B_C}(t)$:

$$F_{B_D}(t) = -6\pi\mu_u r_B(t)\frac{dR_B}{dt} \tag{2.30}$$

$$F_{B_C}(t) = M_B R_B(t)\Omega_0^2 \tag{2.31}$$

where M_B is the mass of the hydrogen bubble, which is a fixed quantity.

The general form of drag on a sphere described by Stoke's Law consists of two components: a normal force F_{B_n} due to pressure acting perpendicularly to the surface, and a tangential force F_{B_t} due to shear stress.

$$F_{B_D} = F_{B_n} + F_{B_t}$$
$$F_{B_n} = -2\pi\mu_u r_B(t)\frac{dR_B}{dt}$$
$$F_{B_t} = -4\pi\mu_u r_B(t)\frac{dR_B}{dt}$$

If we neglect tangential drag, as the bubble sphere surface is gas and it is also assumed that there is no relative motion in the tangential direction between the bubble and the uranium layer ($v_{\theta_u} = v_{\theta_B} = \Omega r$), (2.30) reduces to drag due to pressure:

$$\Rightarrow F_{B_D}(t) = -2\pi\mu_u r_B(t)\frac{dR_B}{dt} \tag{2.32}$$

Adding equations (2.29)-(2.32), we now have the total radial force on the bubble:

$$F_B(t) = F_{B_P}(t) + F_{B_D}(t) + F_{B_C}(t) \tag{2.33}$$

Now we can write Newton's second law governing the bubble's radial motion:

$$M_B\frac{d^2R_B}{dt^2} = F_B(t) \tag{2.34}$$

$$M_B = \rho_0 V_B(t=0)$$
$$M_B = \left(\frac{P_0}{ZR_{H_2}T_0}\right)\left(\frac{4}{3}\pi\right)r_{B_0}^3 \tag{2.35}$$

As (2.34) contains both $R_B(t)$and $r_B(t)$, we can revisit the Young-Laplace equation (2.4):

$$r_B(t) = \frac{2\sigma_{st}}{P_B(t) - P_u(R_B(t))} \tag{2.36}$$

The initial bubble radius r_{B_0} can be found from Blottner[12] and simultaneously solving for Ω_0 by utilizing the Young-Laplace equation at the solid/liquid uranium interface, setting $R_B(0) = r_{u_f}$, and $P_B(R_B(0)) = P_{B_0}$:

$$r_B = C * A$$

where $C = 3.97$ and A is the Laplace constant:

$$A = \left[\frac{\sigma_{st}}{g(\rho_l - \rho_g)}\right]^{1/2}$$

where $g = R_B(t){\Omega_0}^2$, $\rho_l = \rho_u$, and $\rho_g = \rho_B$.

$$\begin{cases} r_{B_0} = C * \left[\dfrac{\sigma_{st}}{r_{uf}{\Omega_0}^2(\rho_u(r_{uf}) - \rho_{B_0})}\right]^{1/2} & \text{(2.37a)} \\ P_{B_0} - P_u(r_{u_f}, \Omega_0) = \dfrac{2\sigma_{st}}{r_{B_0}} & \text{(2.37b)} \end{cases}$$

$P_B(t)$ can be found via (2.36):

$$M_B = \left(\frac{P_B(t)}{ZR_{H_2}T_B(t)}\right)\left(\frac{4}{3}\pi\right) r_B^3(t)$$

$$P_B(t) = \frac{3M_B R_{H_2} Z T_B(t)}{4\pi r_B^3(t)} \tag{2.38}$$

Plugging (2.38) back into (2.36) yields:

$$r_B(t) = \frac{2\sigma_{st}}{\frac{C_0 Z T_B(t)}{r_B^3(t)} - P_u(R_B(t))} \tag{2.39}$$

where $C_0 = \frac{3M_B R_{H_2}}{4\pi}$

Equation (2.39) describes the bubble growth, and requires both $R_B(t)$ and $T_B(t)$. Thus, $r_B(t)$, $R_B(t)$, and $T_B(t)$ are all coupled.

2.5 Final Model

Putting everything together, this model seeks to simultaneously calculate $T_u(r)$, $\rho_u(r)$, $P_u(r)$, $T_B(t)$, $\rho_B(t)$, $P_B(t)$, $R'_B(t)$, $R_B(t)$, and $r_B(t)$ given the following governing equations:

(2.1) $c_{p_B}\frac{d}{dt}(\rho_B T_B) = h[T_u(R_B(t)) - T_B(t)]4\pi r_B^2(t)$

(2.8) $\frac{d^2T_u}{dr^2} + \frac{1}{r}\frac{dT_u}{dr} + \frac{\dot{S}(r)}{K_u} = 0$

(2.10) $\frac{1}{r}\frac{d}{dr}\left(r\frac{du_\theta}{dr}\right) - \frac{u_\theta}{r^2} = 0$

(2.12) $-\rho_u\frac{u_\theta^2}{r} = -\frac{\partial P_u}{\partial r}$

(2.33)
$$F_B(t) = -\int_0^{r_B(t)}\left[\frac{dP_u(r)}{dr}|_{r=R_B(t)+r'} + \frac{P_u(r)|_{r=R_B(t)+r'}}{R_B(t)+r'}\right]4\pi {r'}^2 dr' - 2\pi\mu_u r_B(t)\frac{dR_B}{dt} + M_B R_B(t)\Omega_0^2$$

(2.34) $M_B\frac{d^2R_B}{dt^2} = F_B(t)$

(2.39) $r_B(t) = \frac{2\sigma_{st}}{\frac{C_0 Z T_B(t)}{r_B^3(t)} - P_u(R_B(t))}$

The governing equations lead to the following system of nonlinear ODEs:

$$\begin{cases}
R''_B = \dfrac{F_B(t)}{M_B} & (2.40a)\\[2ex]
P'_B = \dfrac{3h\left[T_u(R_B(t)) - T_B(t)\right]}{r_B(t)\left[\frac{c_{p_B}}{ZR_{H_2}} - 1\right]} & (2.40b)\\[2ex]
r'_B = \dfrac{-2\sigma_{st}}{\left[P_B(t) - P_u(R_B(t))\right]^2}\left[P_B(t) - R'_B\dfrac{dP_u}{dR_B}\right] & (2.40c)\\[2ex]
\rho'_B = \dfrac{-3C_0}{R_{H_2}}\dfrac{r'_B}{r_B(t)^4} & (2.40d)\\[2ex]
T'_B = \dfrac{h\left[T_u(R_B(t)) - T_B(t)\right]4\pi r_B(t)^2 + P'_B V_B(t)}{c_{p_B}M_B} - \dfrac{\rho'_B}{\rho_B(t)}T_B(t) & (2.40e)
\end{cases}$$

2.6 Nuclear & MCNP

As the CGCR is a nuclear reactor, it is necessary to adhere to the design parameter of being in a critical state. That is to say that the effective multiplication factor, k_{eff}, determined by the six factor formula is equal to 1:

$$k_{eff} = \frac{\text{neutrons produced by fission in one neutron generation}}{\text{number of neutrons lost through absorption in the preceding neutron generation}}$$

$$k_{eff} = \eta \cdot \varepsilon \cdot p \cdot f \cdot P_f \cdot P_t$$

where $\eta, \varepsilon, p, f, P_f$, and P_t represent the reproduction factor, fast fission factor, resonance escape probability, thermal utilization factor, fast non-leakage probability, and thermal non-leakage probability, respectively.

The reproduction factor is defined as the ratio of the number of fast neutrons produced by thermal fission to the number of thermal neutrons absorbed in the fuel, which determines the number of neutrons created in the new generation. The fast fission factor is defined as the ratio of the fast neutrons produced by fissions at all energies to the number of fast neutrons produced in thermal fission. The resonance escape probability is the probability that a neutron will be slowed to thermal energy and will escape resonance capture. The thermal utilization factor is the fraction of the thermal neutrons that are absorbed in the nuclear fuel. The fast non-leakage factor is defined as the ratio of the number of fast neutrons that do not leak from the reactor core during the slowing down process to the number of fast neutrons produced by fissions at all energies. And last but not least, the thermal non-leakage factor is defined as the ratio of the number of thermal neutrons that do not leak from the reactor core during the neutron diffusion process to the number of neutrons that reach thermal energies.

If $k_{eff} > 1$, then the reactor is supercritical and the number of neutrons is increasing exponentially in time. If $k_{eff} < 1$, then the reactor is subcritical and the number of neutrons is decreasing and therefore the chain reaction will never be self-sustaining.

The other critical relation necessary in this problem is nuclear heating, or the nuclear energy deposition rate [13][14]:

$$E_d = \frac{N}{V\rho} \int_V \int_t \int_E H(E)\Phi(\vec{r}, E, t) dE dt dV \tag{2.41}$$

Where N and ρ are the atomic and mass densities, respectively, H(E) is the heating response, and $\Phi(\vec{r}, E, t)$ is the particle flux. Energy deposition is in units of MeV/g. Energy deposition will be utilized for the nuclear heating term in (2.8) by scaling the raw F6 tally by the mass density of the material and by a scalar quantity C_i which has units [1/s] and is determined by the power normalization given by[13]:

$$\begin{gathered} Q_i = E_{d_i} \rho_i C_i [Watts/cm^3] \\ ReactorPower = Q_{tot} = \sum_{cells} Q_i V_i \end{gathered} \tag{2.42}$$

The normalization factor can be determined by:

$$NormKCODE = \frac{\nu Q_{tot}}{(1.602 * 10^{-13}) Q_{fis} k_{eff}} \tag{2.43}$$

where ν, and Q_{fis} are the average number of neutrons per fission, and recoverable energy per fission in MeV/fission, respectively, and the units of (2.43) are (kcode source neutrons)/second. From (2.43):

$$E_d = NormKCODE * F_6 \tag{2.44}$$

Both k_{eff} and energy deposition can be calculated via radiation transport utilizing the Monte Carlo N-Particle transport package MCNP v.6.1 [14]. This package is capable of Continuous Energy neutron and photon transport. Interaction probabilities are derived from experimentally obtained nuclear physics cross section data when available.[13] MCNP allows the problem domain to be spatially discretized for reaction rate tallying. For example, this would enable the end user to obtain an estimate for the local energy deposition inside a given volume embedded in the model. The KCODE mode will be used to solve for k_{eff} and the energy deposition rate in equation (2.41) will be determined by the F6 tally in MCNP.

The problem domain within MCNP is geometrically discretized into cells defined by Boolean combinations of spatial regions. Each cell must be defined spatially, as well by characteristic material, density, and particle importance in said cells and can be seen in the input file in Appendix B.1. The CGCR designed in MCNP can be seen in Figures 2.2 & 2.3. To be noted, the uranium region (in blue) has been subdivided into 1mm increments due to the varying density profile.

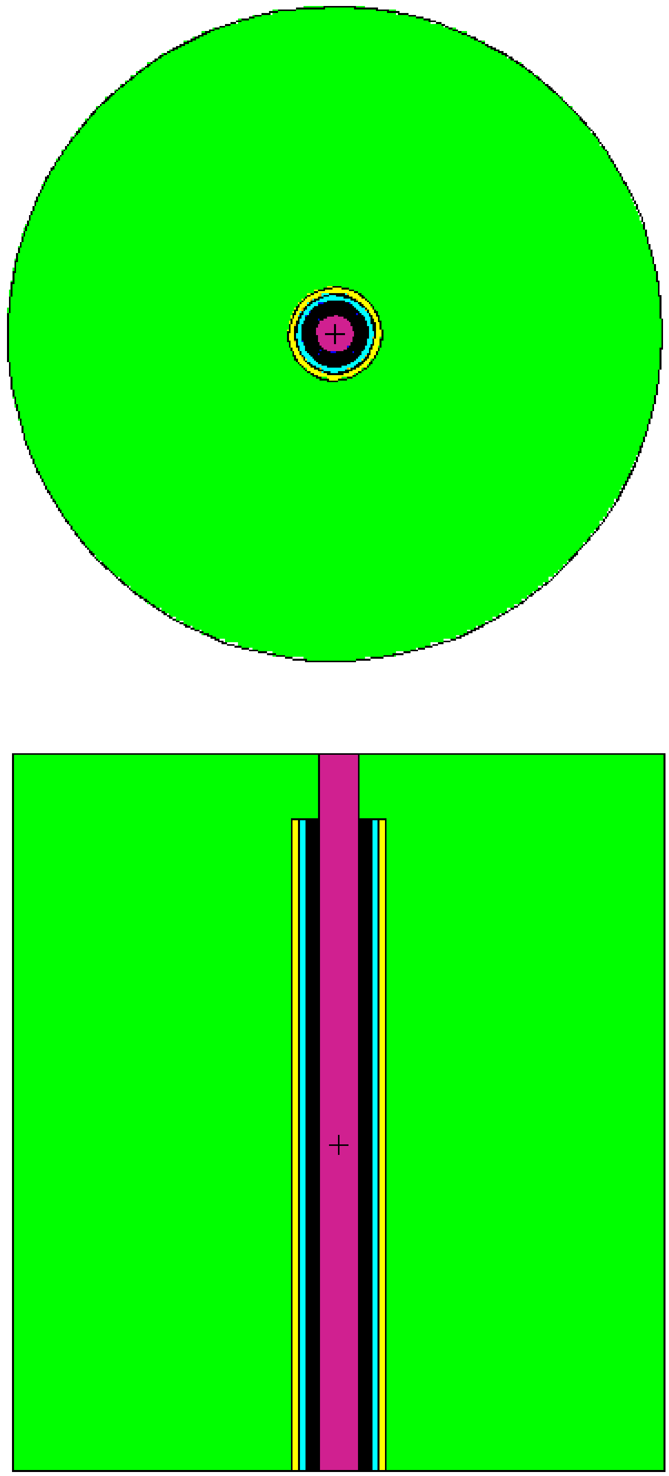

Figure 2.2: Reactor top & side cross-section centrifugal region, as designed in MCNP. Green = Beryllium, Yellow = Li_7H, Orange = cold H_2, Light Blue = Graphite frit, Blue = Uranium, Purple = hot H_2

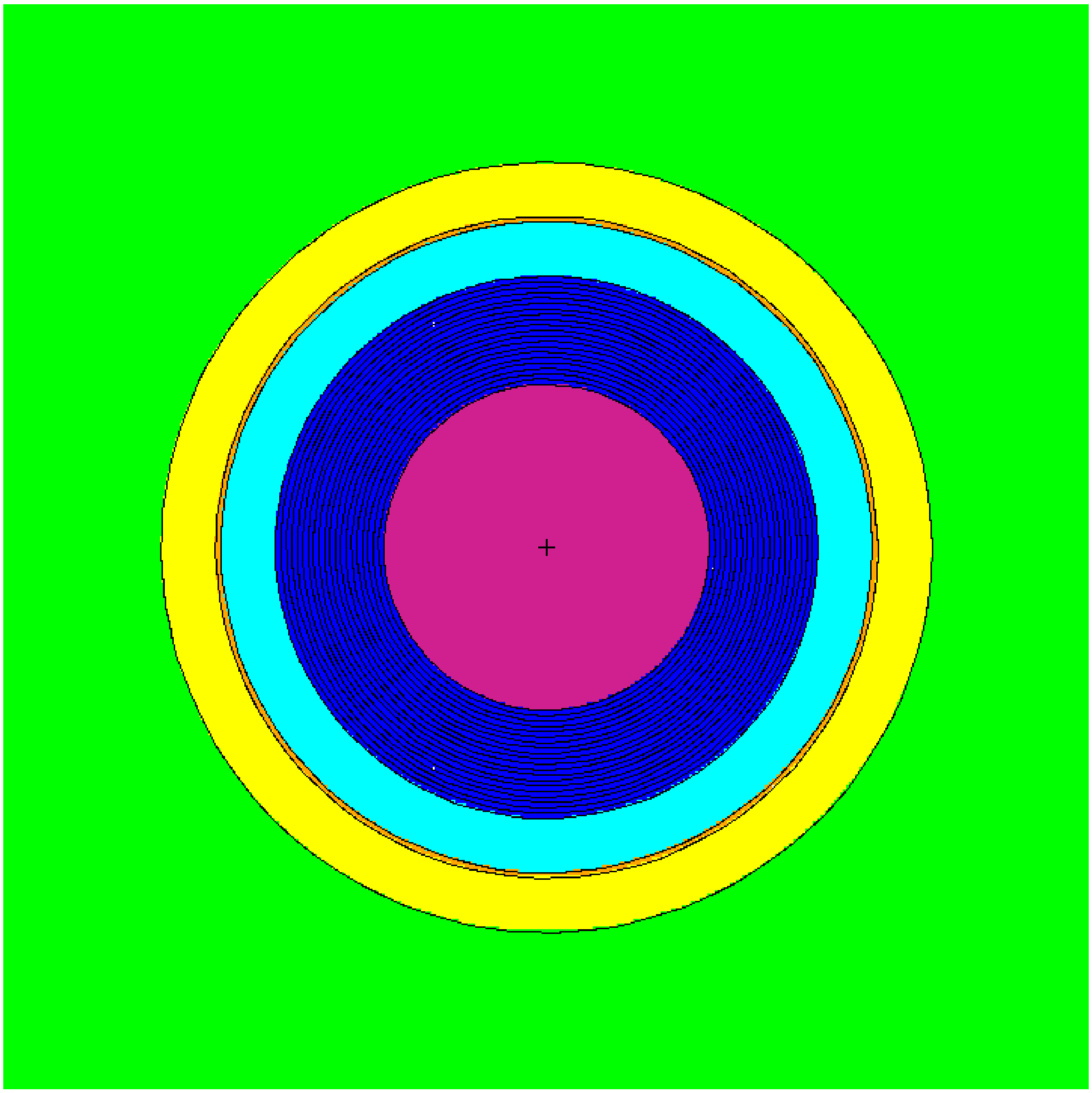

Figure 2.3: Reactor top cross-section centrifugal region, as designed in MCNP. Green = Beryllium, Yellow = Li_7H, Orange = cold H_2, Light Blue = Graphite frit, Blue = Uranium, Purple = hot H_2

CHAPTER 3: RESULTS

Utilizing analytical and numerical methods via Mathematica and MATLAB, as well as an initial reactor designed and analyzed in MCNP, a cyclic iteration method was utilized to determine temperature, density, and pressure profiles of the uranium layer $(T_u(r), \rho_u(r), P_u(r))$. The initial parameters were chosen to be as follows:

Table 3.1: Initial Parameters[1]

$T_u(r = r_u) = 800$ K	$r_u = 5$ cm	$K_u = 27$ W/m K
$T_{u_{fus}} = 1405.3$ K	$r_p = 3$ cm	$Q_{tot} = 10$ MW
$T_{u_{vap}} = 4404$ K	$H = 100$ cm	$Q_{fis} = 200$ MeV/fission
$T_u(r = r_p) = 5500$ K	$\mu_u = 6.5$ cP	$\rho_{u_s} = 19100$ kg/m^3
$T_{B_0} = T_{u_{fus}}$	$\rho_{B_0} = 5$ kg/m^3	$\rho_{B_{max}} = 10000$ kg/m^3
$h = 1000$ W/m^2K	$\dot{m}_{H_2} = 0.05$ kg/s	$\sigma_{st} = 1500$ dyne/cm
$c_{p_B} = 18000$ J/kg-K	$R_{H_2} = 4124$ kg/mol	$R_u = 34.9328$ kg/mol
$T_{crit_{H_2}} = 33.2$ K	$P_{crit_{H_2}} = 12.797$ atm	$P_0 = 30$ MPa

The effective multiplication factor, k_{eff}, was found to have a value of 0.884 ± 0.001, and the raw energy deposition F_6 was found to have a mean of 7.254e-04 MeV/g $\pm$ 6.833e-04 MeV/g. From the temperature profile and melting and boiling points of uranium in Figure 3.1, the locations of uranium phase change were determined to be $r_{u_f} \approx 0.0468m$ and $r_{u_v} \approx 0.0338m$. From the density profile in Figure 3.2, the mass of the uranium in the finite cylinder of height $H = 100cm$ was found to be 69.114kg. For multiples of Ω_0 (5,10,15,20), density profiles were fed back into MCNP to find corresponding $k_{eff} =$ 0.89812, 0.93220, 0.95964, 0.96092. This can be seen in Figures 3.3 & 3.4. From the density profile, the pressure profile was determined and is shown in Figure 3.5. The optimum angular velocity (Ω_0) for this setup was determined to be 1605.36 Hz. This was found by utilizing equation (2.37).

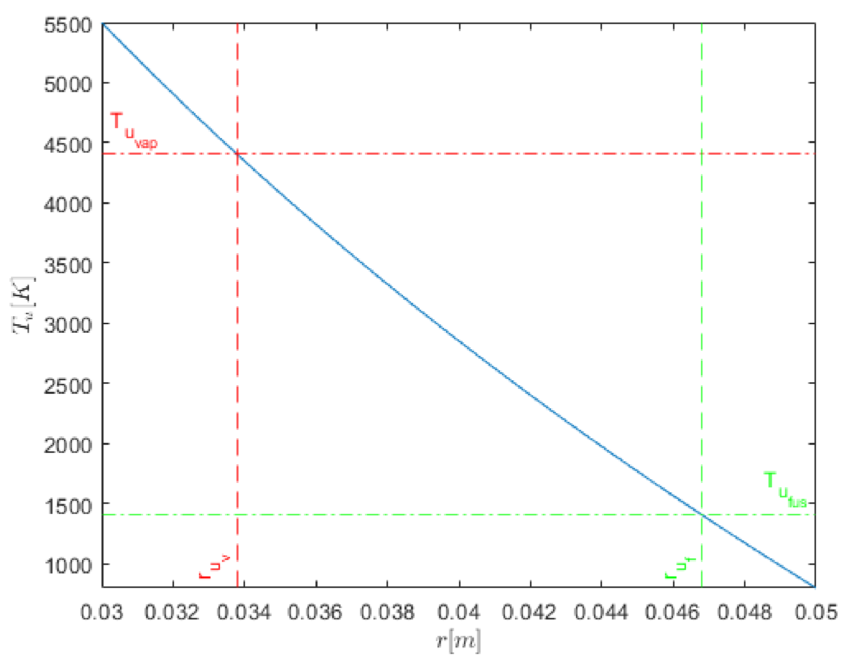

Figure 3.1: Radial temperature profile T_u within uranium layer. Melting and boiling temperatures of uranium are included to show the location of phase change.

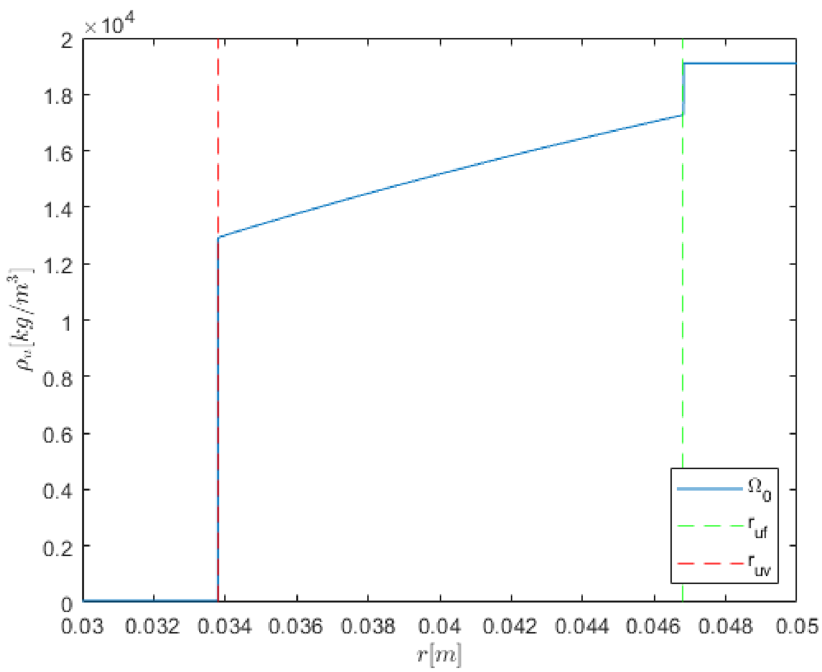

Figure 3.2: Radial density profile ρ_u for $\Omega_0 \approx 1605$ Hz

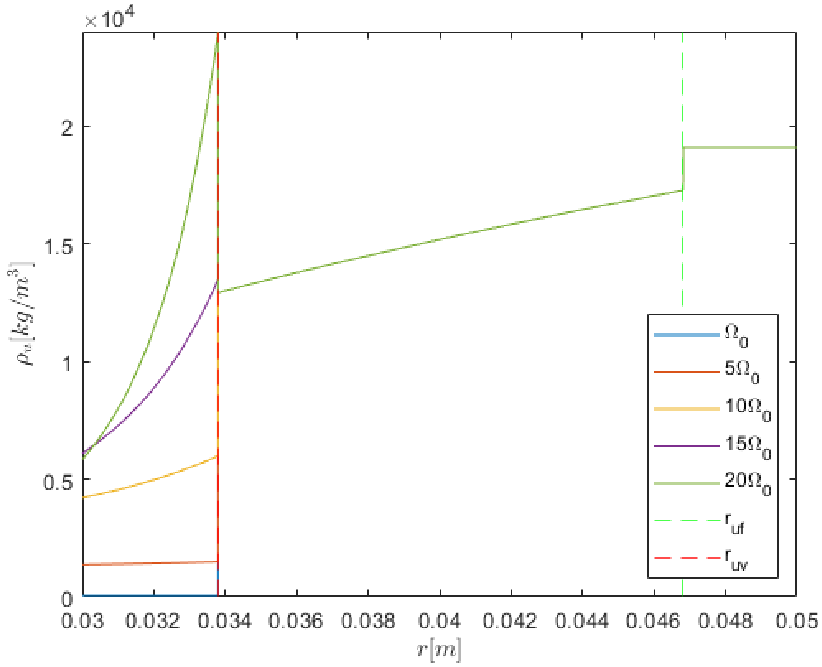

Figure 3.3: Radial density profile ρ_u for various angular velocities. Increasing angular velocity (Ω) results in an increased density shift radially outwards in the vapor region, as expected.

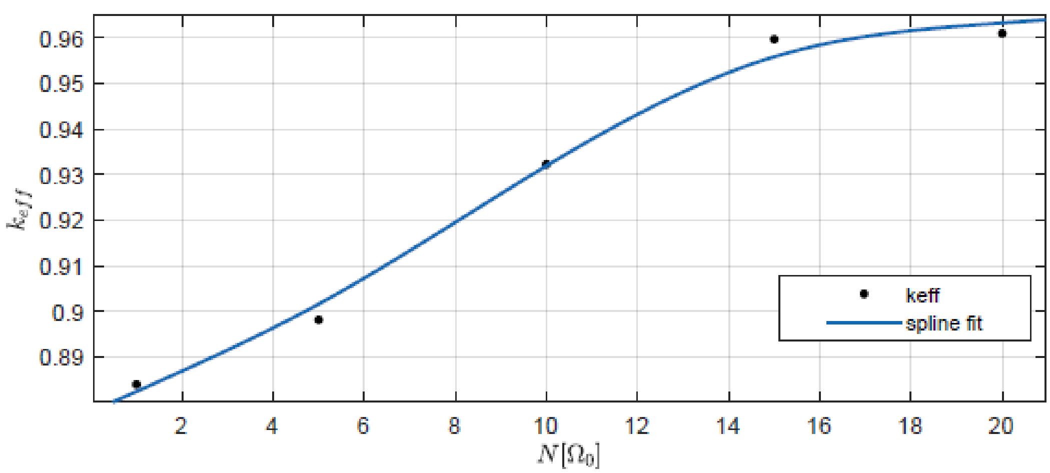

Figure 3.4: k_{eff} vs. various multiples of Ω_0. This shows that k_{eff} increases with increasing angular velocity as more mass is allowed in uranium vapor layer.

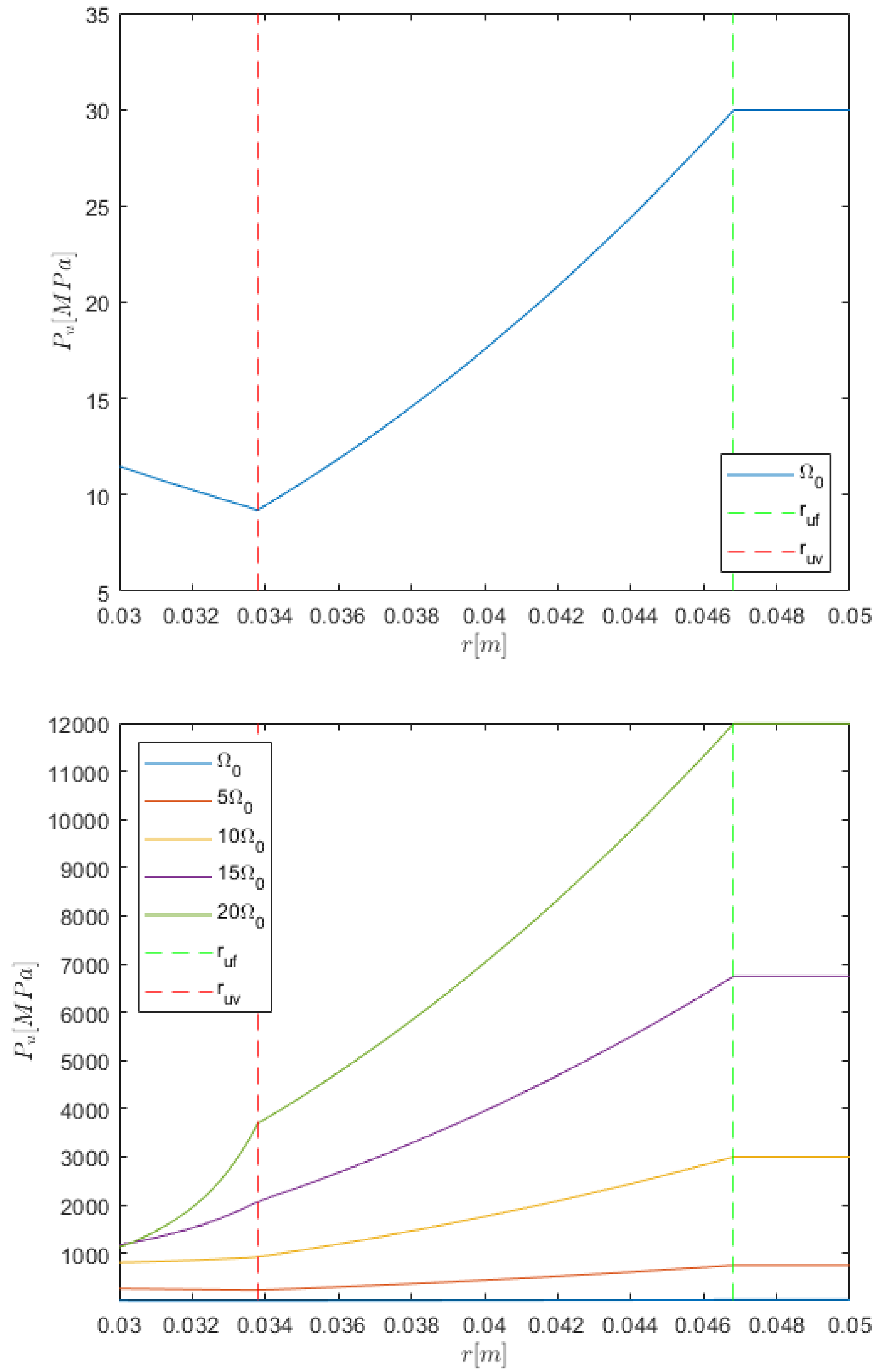

Figure 3.5: Top: Radial pressure profile P_u for $\Omega_0 \approx 1605$ Hz. Bottom: Radial pressure profile P_u for various angular velocities. Increasing angular velocity (Ω) results in an increased pressure shift radially outwards in the vapor region, as well as increased pressure throughout the liquid region, as expected.

From the real gas equation (2.2) and Table 3.1, $Z_0 = 1.0353$. Given conservation of mass and Table 3.1, Initial velocity $R'_B(0) = -\dot{m}_{H_2}/(2\pi H r_{uf} \rho_{B_0}) \approx -0.034$m/s. Initial bubble radius $r_{B_0}$is calculated to $\approx 101.3\mu$m. As the bubble is injected radially inward, the solution to ODEs (2.40) suggest an immediate drop in bubble temperature and bubble radius as the bubble compresses to a minimum size $r_{B_{min}} = 8.04\mu$m limited by $\rho_{B_{max}}$, which was chosen to be on the order of metallic hydrogen assuming fusion doesn't occur. By the time the bubble traverses the liquid uranium layer and reaches r_{uv}, $t = 2.0881$ ms, $R'_B = -3.0856$m/s, $P_B = 834.795$ MPa, and $T_B = 18.3421$ K. The trends can be seen in Figures 3.6-3.10.

Looking to the bubble evolution described by the governing equations (2.1)-(2.40) and the figures in the previous chapter, it can be noted the second term in equation (2.40e) is dominant until $\rho_{B_{max}}$ is reached and $\rho_B(t)' \Rightarrow 0$; once this occurs, the second term vanishes, causing $T_B(t)'$ to become positive. Once the hydrogen bubble fully compresses, the centrifugal term in equation (2.40a) becomes dominant, thus decelerating the bubble. This therefore shows logical consistency between the bubble evolution equations and figures.

As an extension of this study, for comparison with the preliminary reference design in Figure A.1, this single fuel element design was also made into a lattice structure of 13 elements, as seen in Figure 3.11. This lattice resulted in an expected increased $k_{eff} = 1.190 \pm 0.001$.

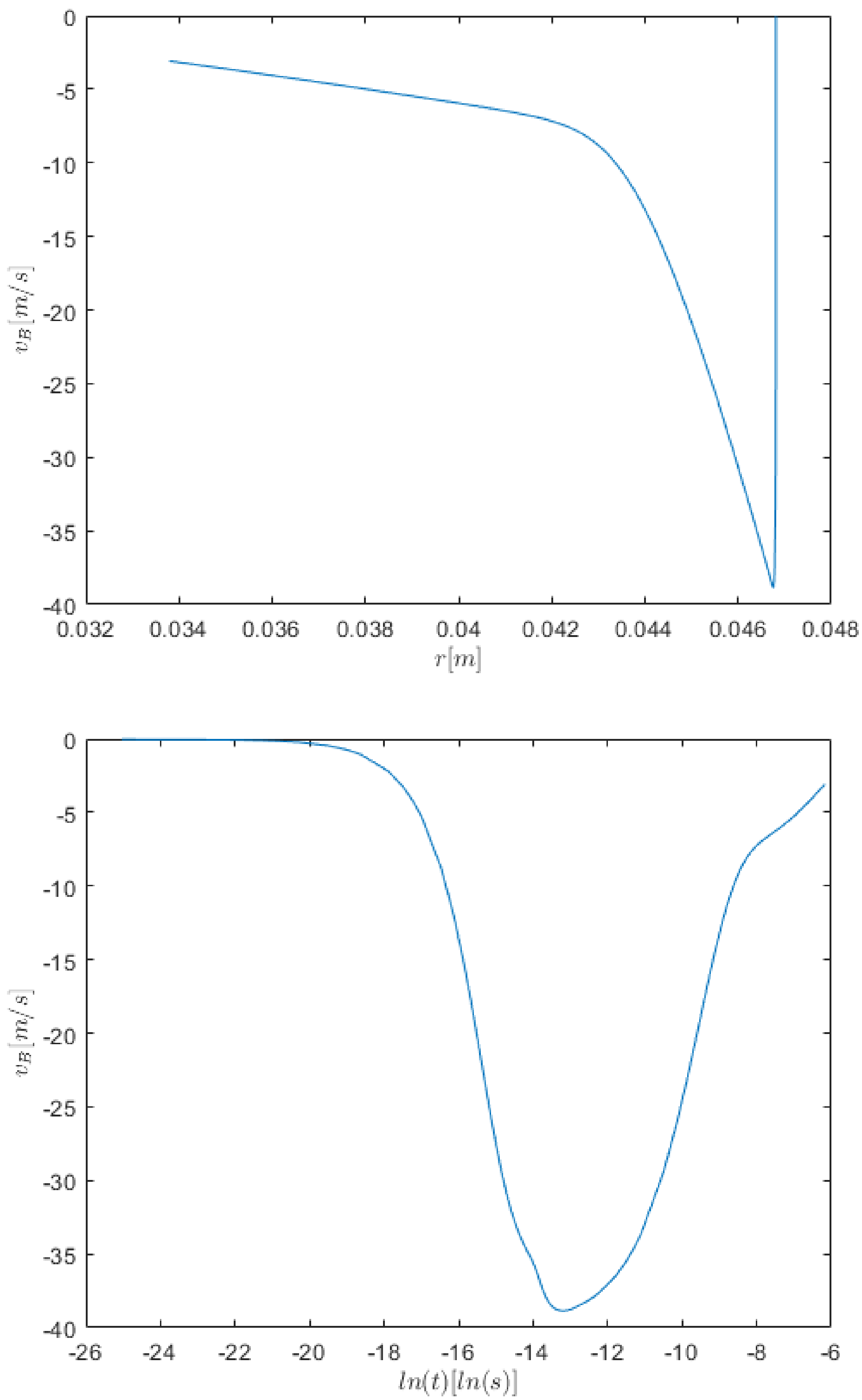

Figure 3.6: Top: Radial bubble velocity v_B vs. radial position r for $\Omega_0 \approx 1605$ Hz. Bottom: Radial bubble velocity v_B vs. $ln(t)$ for $\Omega_0 \approx 1605$ Hz. Indicates the bubble accelerates rapidly during compression and then decelerates once minimum radius is reached.

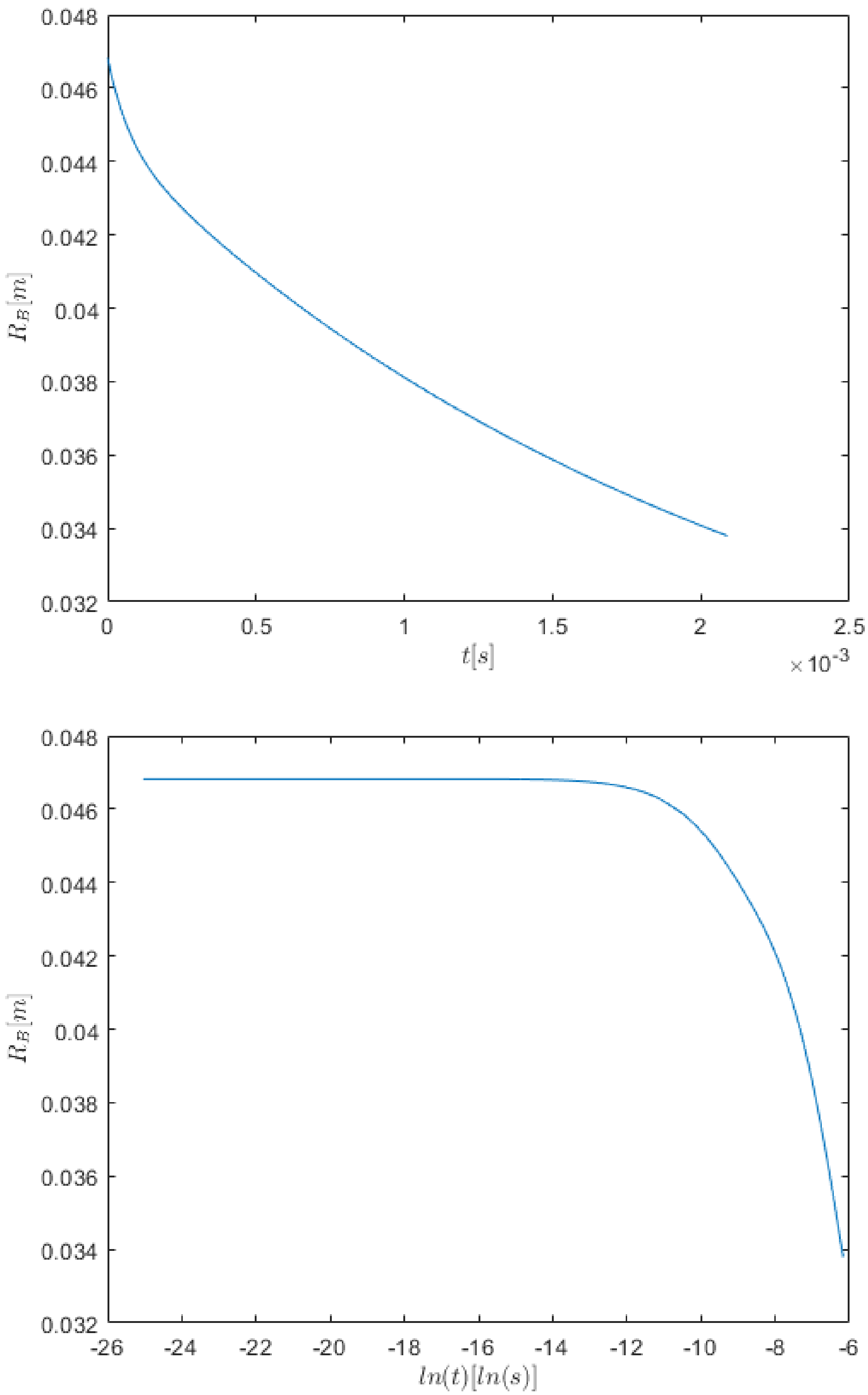

Figure 3.7: Top: Radial bubble position R_B vs. t, for $\Omega_0 \approx 1605$ Hz.
Bottom: Radial bubble position R_B vs. $ln(t)$, for $\Omega_0 \approx 1605$ Hz.

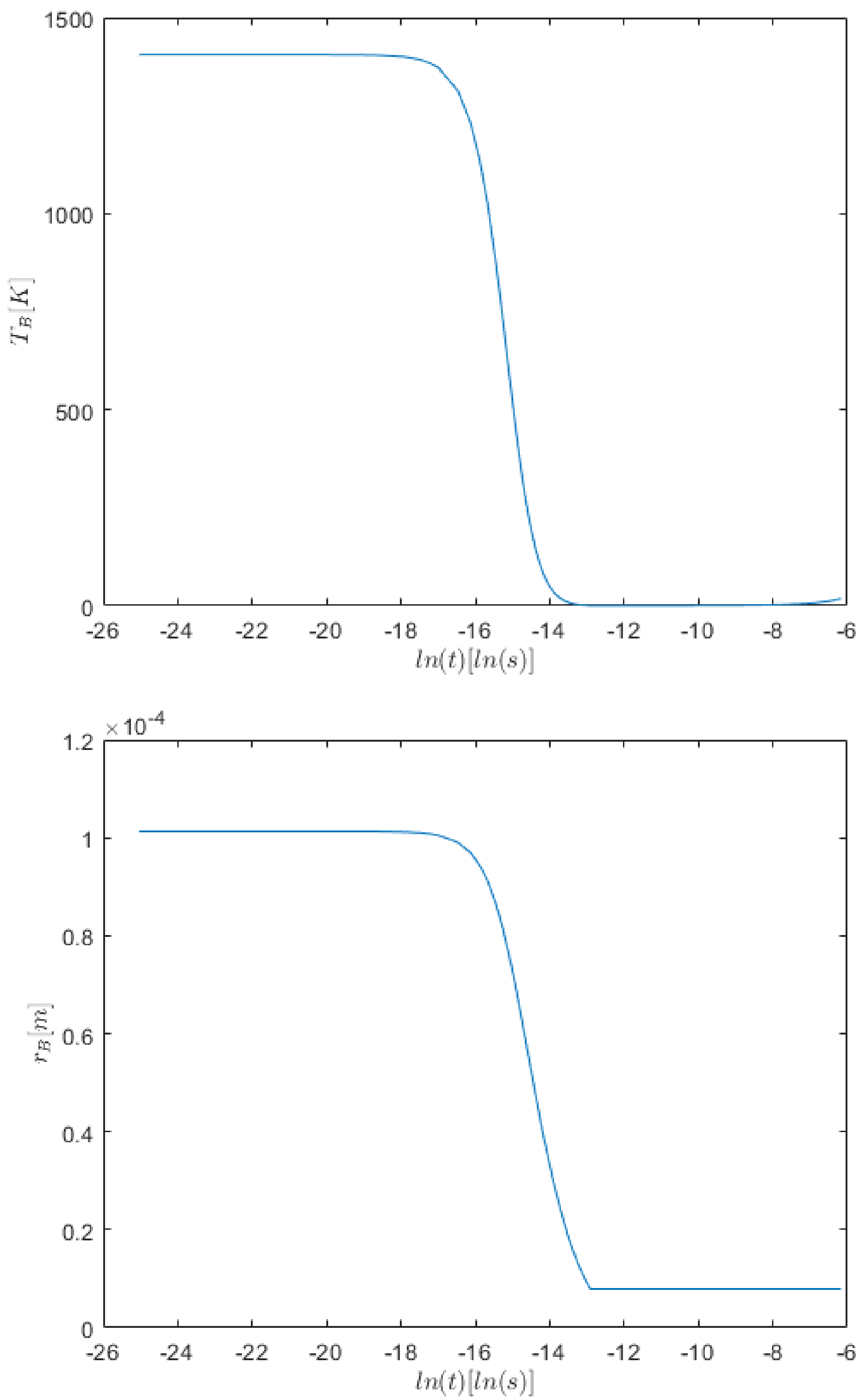

Figure 3.8: Top: Bubble temperature T_B vs. $ln(t)$, for $\Omega_0 \approx 1605$ Hz. Bubble initially compresses and super-cools to a minimum temperature $T_{B_{min}} \approx 0.6591$ K, and then increases to 18.3421 K. Bottom: Bubble radius r_B vs. $ln(t)$, for $\Omega_0 \approx 1605$ Hz. Bubble initially compresses to a minimum radius $r_{B_{min}}$ and then remains constant.

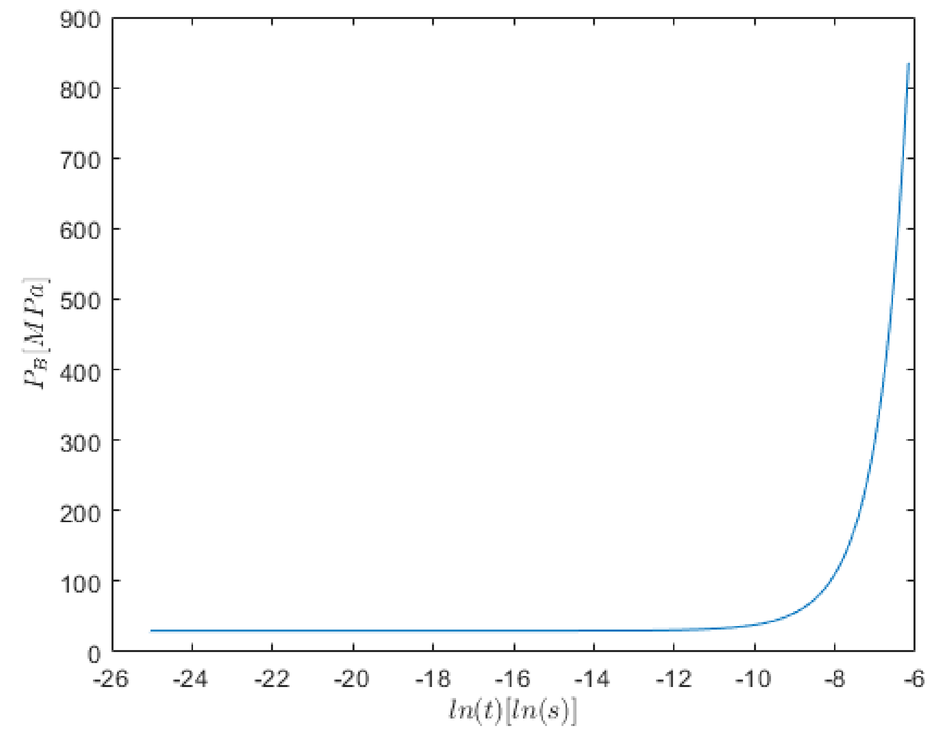

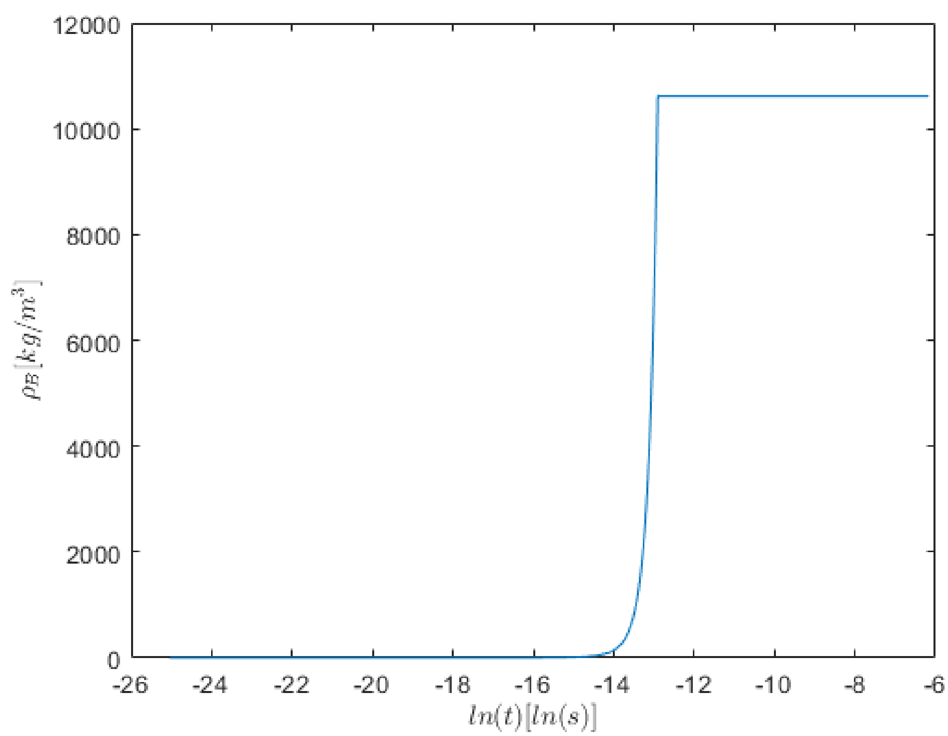

Figure 3.9: Top: Bubble pressure P_B vs. $ln(t)$, for $\Omega_0 \approx 1605$ Hz. Bubble pressure increases as it moves radially inward. Bottom: Bubble density ρ_B vs. $ln(t)$, for $\Omega_0 \approx 1605$ Hz. Bubble initially compresses to a maximum density $\rho_{B_{max}}$ and then remains constant.

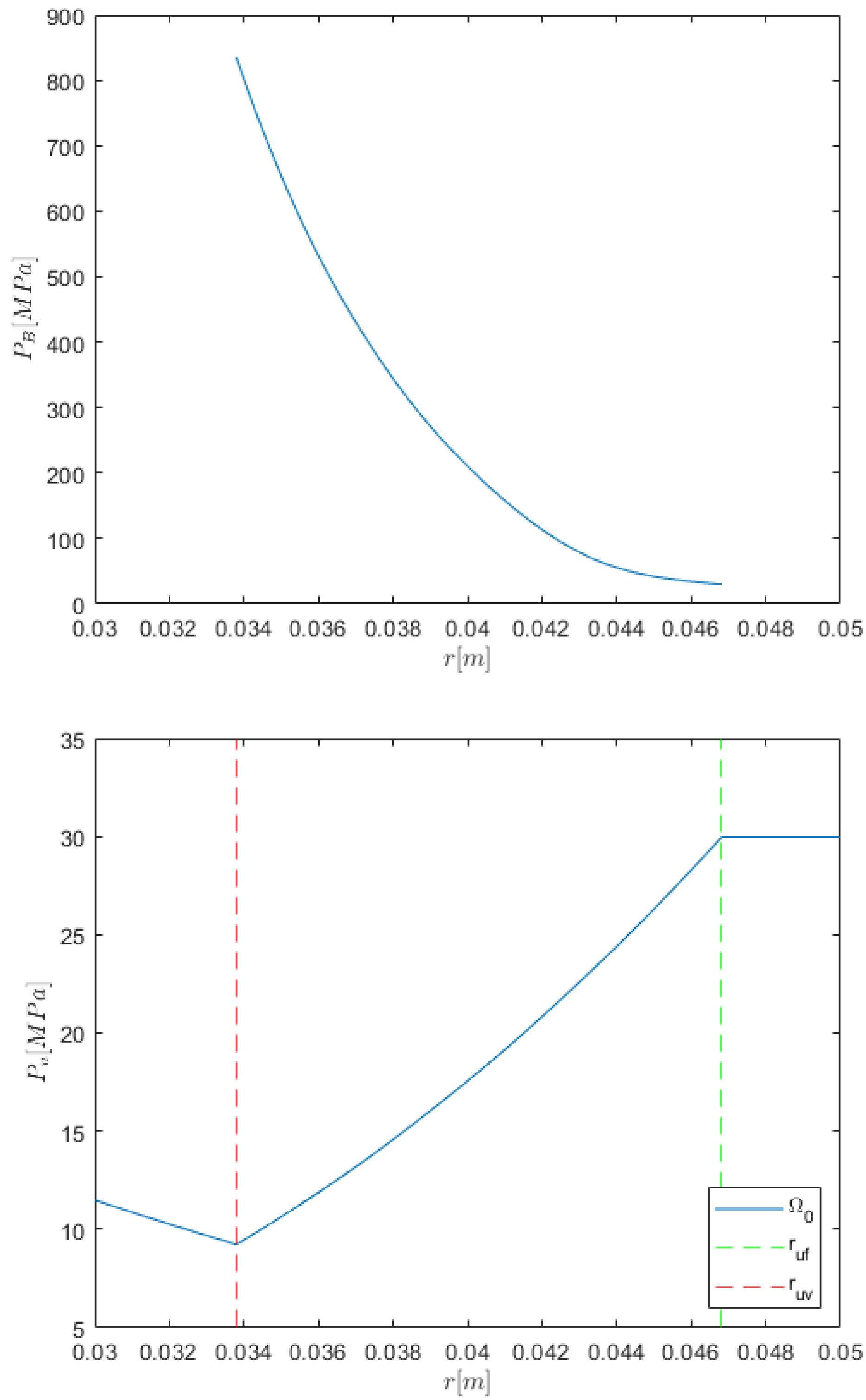

Figure 3.10: Bubble pressure P_B vs. radial position r, for $\Omega_0 \approx 1605$ Hz. Bottom: Uranium layer pressure P_u vs. radial position r, for $\Omega_0 \approx 1605$ Hz.

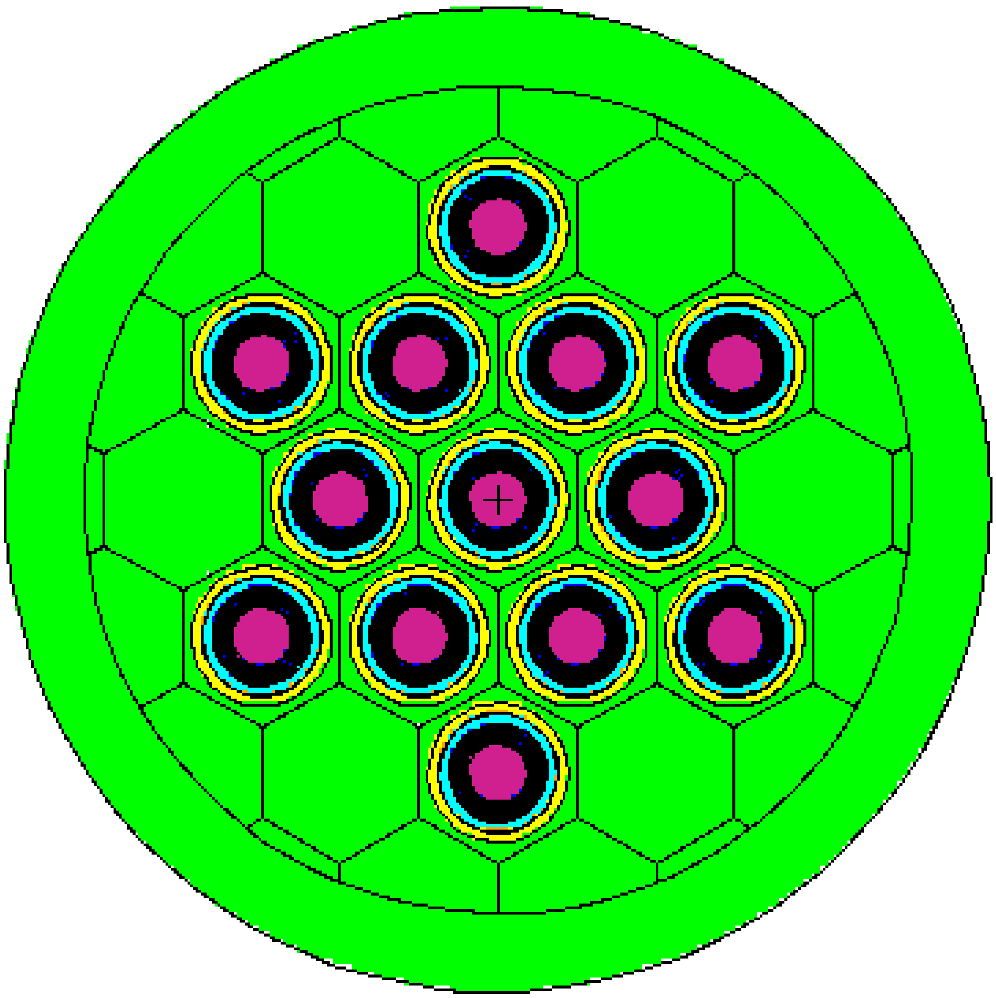

Figure 3.11: Reactor with 13 fuel elements

CHAPTER 4: DISCUSSION AND FURTHER STUDY

Results in the previous chapter suggest that centrifugal separation of uranium and hydrogen will be beneficial. It can also be noted that in Figure 3.3 varying angular velocity will change the density at the liquid/gas uranium interface, as well as indicating that for a constant mass system, r_p will vary with varying angular velocity. However, when looking at the pressure profile in Figure 3.5 and the Young-Laplace relation (2.4), we can see that the angular velocity is limited by the initial input pressure provided by the NTRs propellant turbopump as well as current centrifugal technology. A turbopump is necessary to reduce the mass and thickness of the hydrogen pressure tank wall while achieving the required operational pressures for high performance and thrust of the rocket. Pressures above 30 MPa are currently outside of current turbopump capabilities, however, when looking at the trend of bubble pressure within the liquid uranium layer, the potential for utilizing this behavior in dense liquids to step up the pressure could be studied in the future. However, this also relies on the improvement of centrifugal technology; magnetic bearings currently are seeing rpm values of 500,000 (=8333 Hz). Minor variation in angular velocity may provide significant control over the dynamics of the uranium gas region; varying angular velocity would result in the change in plenum location r_p, as well as allow for the possibility of turning the mass flow rate off/on by increasing/decreasing $P_u(ruf, \Omega)$ above/below the input hydrogen pressure. The results of the bubble evolution suggest that this technique may also be able to produce metastable metallic hydrogen, which is a more efficient propellant, that reaches the reaction chamber.

Further study may be required to numerically solve for equation (2.8) with varying $E_d(r)$. As the bulk density of uranium and hydrogen seemed negligibly different, the uranium region was treated as purely uranium; however, further study may be required in regards to accurate mass fractions and porosity of the uranium layer. As the hydrogen bubble reaches the uranium vapor layer, two possible scenarios arise: either (1) the bubble disperses and becomes well-mixed in the uranium layer, in which a diffusion model may be necessary for future study, or (2) the bubble disperses into a column/finger spanning the thickness of the vapor layer, in which a jet model may be in order. Further optimization of design parameters could be done to minimize critical mass and maximize thermal coupling between nuclear fuel and propellant, for comparison to other reactors.

Although the design parameters for the model of a single fuel element resulted in a subcritical state ($k_{eff} < 1$), an expanded lattice structure of 13 elements was tested with the designed density profiles resulting in a supercritical state ($k_{eff} > 1$). A higher k_{eff} for a multi-element reactor is to be expected, as there is more fissionable material for neutrons from each element to interact with; however, both subcritical and supercritical states are not desired for a self-sustaining reactor. Therefore continued iteration and optimization with the lattice structure is necessary to find a convergence of the density profile and k_{eff}=1. Additional study of various moderator distributions may also prove beneficial to reactor performance. This could be achieved by seeding the hydrogen propellant with a moderator, by using a temporary "hot frit" that melts/vaporizes and mixes with the uranium fuel upon start-up, by using similar fuel pellets used in PBRs, or a combination thereof.

As this design is highly conceptual, many assumptions will need to be revisited in future models to address thermal properties that vary with temperature. Due to limited data on the thermal properties of high temperature (gaseous) uranium, future experimentation to extend the knowledge base of uranium thermal properties is required to advance the accuracy of this model. Additional study may also investigate the system of mostly gaseous uranium, however such a system may be unstable due to plasma ionization and potential magnetohydrodynamic instabilities. This research may also extend to other fluid system applications outside of NTP. The successful conclusion of this research has been to demonstrate a first model of CGCR using low enriched uranium metal, centrifugal separation, and fuel/propellant heat transfer.

REFERENCES

[1] Y. Ji, Z. Liu, J. Sun, and L. Shi, "Analysis of the Flow Distribution in a Particle Bed Reactor for Nuclear Thermal Propulsion," *Energies*, vol. 12, pp. 1–19, September 2019.

[2] M. Houts, "High Performance NTP," March 2020.

[3] H. F. Bauer, "Rotating finite liquid systems under zero-gravity," *Forschung im Ingenieurwesen*, vol. A, no. 48, pp. 169–179, 1982.

[4] M. Houts, "Potential NTP Research Benefits," November 2019.

[5] M. Houts and S. Mitchell, "Development and Utilization of Nuclear Thermal Propulsion," 2016.

[6] B. Spriet, "Surface tension of uranium and plutonium at the melting point," *Mem. Sci. Rev. Met.*, vol. 60, 1963.

[7] J. Cahill and A. Kirshenbaum, "The surface tension of liquid uranium from its melting point, 1406°K to 1850°K," *Journal of Inorganic and Nuclear Chemistry*, vol. 27, no. 1, pp. 73–76, 1965.

[8] J. D. Anderson, *Modern Compressible Flow: with Historical Perspective.* McGraw-Hill, third ed., 2003.

[9] R. L. Panton, *Incompressible Flow.* Wiley, fourth ed., 2013.

[10] E. A. Fischer, "Density of Liquid Uranium and Derived Equation of State," February 2000.

[11] R. Mulford and R. Sheldon, "Density and heat capacity of liquid uranium at high temperatures." Journal of nuclear materials. , 1988, Vol.154(2), p.268-275.

[12] F. G. Blottner, "Hydrodynamics and heat transfer characteristics of liquid pools with bubble agitation," tech. rep., Sandia Labs., Albuquerque, NM (USA), 1979.

[13] W. L. Gurecky, "Development of an MCNP6 - ANSYS FLUENT Multiphysics Coupling Capability," 2015.

[14] *MCNP6 Users Manual - Code Version 6.1.1beta*, June 2014. LA-CP-14-00745.

[15] E. W. Lemmon, M. O. McLinden, and D. G. Friend, *NIST Standard Reference Database Number 69, Eds. P.J. Linstrom and W.G. Mallard*, ch. Thermophysical Properties of Fluid Systems. National Institute of Standards and Technology.

[16] D. Ofte, "The viscosities of liquid uranium, gold and lead," *Journal of Nuclear Materials*, vol. 22, no. 1, pp. 28–32, 1967.

APPENDIX A: ADDITIONAL FIGURES

Figure A.1: Preliminary reference design of LEU CGCR with UF_6 as fuel. Analysis done by U-space, provided by NASA

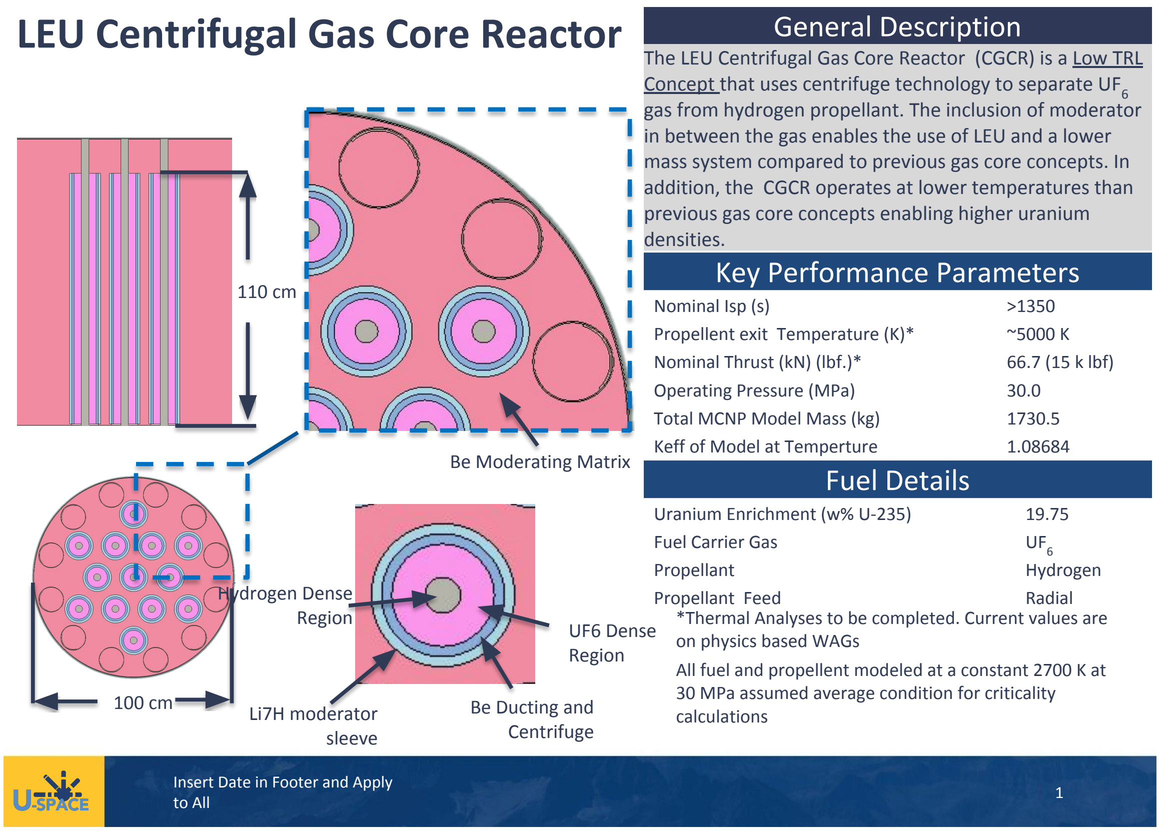

APPENDIX B: PROGRAM FILES

B.1 MCNP INPUT

```
c Cell Cards
1  1   -0.0005061  -1 -26          imp:n,p 1       $ hot h2
2  2   -0.059768    1 -2 -25 -26       imp:n,p 1       $ Uranium metal LEU
3  2   -0.059817    2 -3 -25 -26       imp:n,p 1       $
4  2   -0.059873    3 -4 -25 -26       imp:n,p 1       $
5  2   -2.704474    4 -5 -25 -26       imp:n,p 1       $
6  2   -13.204924   5 -6 -25 -26       imp:n,p 1       $
7  2   -13.585757   6 -7 -25 -26       imp:n,p 1       $
8  2   -13.956008   7 -8 -25 -26       imp:n,p 1       $
9  2   -14.316250   8 -9 -25 -26       imp:n,p 1       $
10  2   -14.667010   9 -10 -25 -26      imp:n,p 1       $
11  2   -15.008775  10 -11 -25 -26      imp:n,p 1       $
12  2   -15.341993  11 -12 -25 -26      imp:n,p 1       $
13  2   -15.667083  12 -13 -25 -26      imp:n,p 1       $
14  2   -15.984431  13 -14 -25 -26      imp:n,p 1       $
15  2   -16.294397  14 -15 -25 -26      imp:n,p 1       $
16  2   -16.597318  15 -16 -25 -26      imp:n,p 1       $
17  2   -16.893506  16 -17 -25 -26      imp:n,p 1       $
18  2   -17.513585  17 -18 -25 -26      imp:n,p 1       $
19  2   -19.100000  18 -19 -25 -26      imp:n,p 1       $
20  2   -19.100000  19 -20 -25 -26      imp:n,p 1       $
21  2   -19.100000  20 -21 -25 -26      imp:n,p 1       $
22  5   -0.85423595     21 -22 -25 -26      imp:n,p 1       $ graphite/H2 ducting
23  6   -0.0084719  22 -23 -25 -26      imp:n,p 1       $ cold h2
24  3       -0.783      23 -24 -25 -26      imp:n,p 1       $ Li7H reflector
c reactor vessel
25  4   -1.85       (24 -26):(1 -24 25 -26) imp:n,p 1       $ Beryllium mod
26  0                26            imp:n,p 0       $ void outside

c Surface Cards
c solution cylinder
1   cz  3.0     $ hot H2/LEU cyl surf
2   cz  3.1
3   cz  3.2
4   cz  3.3
5   cz  3.4
6   cz  3.5
7   cz  3.6
8   cz  3.7
9   cz  3.8
10  cz  3.9
11  cz  4.0
12  cz  4.1
13  cz  4.2
14  cz  4.3
15  cz  4.4
16  cz  4.5
17  cz  4.6
18  cz  4.7
19  cz  4.8
20  cz  4.9
21  cz  5       $ inner porous centrifuge wall surf
22  cz  6       $ outer porous centrifuge wall surf
23  cz  6.1     $ inner reflect surf
24  cz  7.1     $ outer reflect surf
25  pz  50      $ centrifuge top
c reactor vessel
26  rcc     0 0 -50  0 0 110  50        $ outer Mod surf

c Data Cards
mode n p
kcode   5000 1 20 100   $  Calculate keff
ksrc    0 4.05 0
c Materials
M1  1001.84c    1.0     $ Hot H2 @ 2700K
M2  92235.84c   -0.1975     $ LEU w%U-235 19.75
    92238.84c   -0.8025
M3  3007.86c    -0.97988    $ Li7H
        1001.86c    -0.02012
```

```
M4  4009.80c    1.0     $ Beryllium
MT4 be.20t
M5  6000.82c    -0.995041   $ porous(50%) graphite saturated with H2 @900K
    1001.82c    -0.004959
M6  1002.85c    1.0     $ liquid H2
M7  6000.86c    1.0     $ graphite
M7T grph.20t
c Tallies
e0:n    0.1 1.0 20.0        $ Default energy bins (MeV)
f2:n,p  26.1 26.2 26.3 T    $ photon & neutron flux through surface
f4:n    1 2 3 4 5 6 7 8 9 10 11 12 13 14 15         $ flux in cells
    16 17 18 19 20 21 22 23 24 25
f6:n,p  1 2 3 4 5 6 7 8 9 10 11 12 13 14 15 16
    17 18 19 20 21 22 23 24 25  $ energy deposition
```

B.2 MCNP OUTPUT

```
          Code Name & Version = MCNP6, 1.0

     _/      _/        _/_/_/       _/      _/       _/_/_/         _/_/_/
    _/_/  _/_/      _/             _/_/    _/       _/    _/     _/
   _/  _/  _/      _/             _/  _/  _/       _/_/_/       _/_/_/
  _/      _/      _/             _/    _/_/       _/           _/    _/
 _/      _/        _/_/_/       _/      _/       _/             _/_/

  +---------------------------------------------------------------------+
  | Copyright 2008. Los Alamos National Security, LLC.  All rights      |
  | reserved.                                                           |
  |   This material was produced under U.S. Government contract         |
  | DE-AC52-06NA25396 for Los Alamos National Laboratory, which is      |
  | operated by Los Alamos National Security, LLC, for the U.S.         |
  | Department of Energy. The Government is granted for itself and      |
  | others acting on its behalf a paid-up, nonexclusive, irrevocable    |
  | worldwide license in this material to reproduce, prepare derivative |
  | works, and perform publicly and display publicly. Beginning five    |
  | (5) years after 2008, subject to additional five-year worldwide     |
  | renewals, the Government is granted for itself and others acting on |
  | its behalf a paid-up, nonexclusive, irrevocable worldwide license   |
  | in this material to reproduce, prepare derivative works, distribute |
  | copies to the public, perform publicly and display publicly, and to |
  | permit others to do so. NEITHER THE UNITED STATES NOR THE UNITED    |
  | STATES DEPARTMENT OF ENERGY, NOR LOS ALAMOS NATIONAL SECURITY, LLC, |
  | NOR ANY OF THEIR EMPLOYEES, MAKES ANY WARRANTY, EXPRESS OR IMPLIED, |
  | OR ASSUMES ANY LEGAL LIABILITY OR RESPONSIBILITY FOR THE ACCURACY,  |
  | COMPLETENESS, OR USEFULNESS OF ANY INFORMATION, APPARATUS, PRODUCT, |
  | OR PROCESS DISCLOSED, OR REPRESENTS THAT ITS USE WOULD NOT INFRINGE |
  | PRIVATELY OWNED RIGHTS.                                             |
  +---------------------------------------------------------------------+

1mcnp     version 6     ld=05/08/13                    04/27/20 10:00:27

 *************************************************************************
   probid =  04/27/20 10:00:27
 ixr n=INP_U_OD_10_ID_6_dens_prof_pure_vls_4


  warning.  Physics models disabled.
         1-       c Cell
         Cards
         2-       1       1       -0.0005061      -1 -26                  imp:n,p
         1
         3-       2       2       -0.059768        1 -2 -25 -26           imp:n,p
         1
         4-       3       2       -0.059817        2 -3 -25 -26           imp:n,p
         1
         5-       4       2       -0.059873        3 -4 -25 -26           imp:n,p
         1
         6-       5       2       -2.704474        4 -5 -25 -26           imp:n,p
         1
         7-       6       2       -13.204924       5 -6 -25 -26           imp:n,p
         1
         8-       7       2       -13.585757       6 -7 -25 -26           imp:n,p
         1
         9-       8       2       -13.956008       7 -8 -25 -26           imp:n,p
         1
        10-       9       2       -14.316250       8 -9 -25 -26           imp:n,p
        1
        11-       10      2       -14.667010       9 -10 -25 -26          imp:n,p
        1
        12-       11      2       -15.008775      10 -11 -25 -26          imp:n,p
        1
        13-       12      2       -15.341993      11 -12 -25 -26          imp:n,p
        1
        14-       13      2       -15.667083      12 -13 -25 -26          imp:n,p
        1
        15-       14      2       -15.984431      13 -14 -25 -26          imp:n,p
```

```
1
16-      15    2     -16.294397     14 -15 -25 -26          imp:n,p
1
17-      16    2     -16.597318     15 -16 -25 -26          imp:n,p
1
18-      17    2     -16.893506     16 -17 -25 -26          imp:n,p
1
19-      18    2     -17.513585     17 -18 -25 -26          imp:n,p
1
20-      19    2     -19.100000     18 -19 -25 -26          imp:n,p
1
21-      20    2     -19.100000     19 -20 -25 -26          imp:n,p
1
22-      21    2     -19.100000     20 -21 -25 -26          imp:n,p
1
23-      22    5     -0.85423595    21 -22 -25 -26          imp:n,p
1
24-      23    6     -0.0084719     22 -23 -25 -26          imp:n,p
1
25-      24    3     -0.783         23 -24 -25 -26          imp:n,p
1
26-      c reactor
vessel
27-      25    4     -1.85          (24 -26):(1 -24 25 -26) imp:n,p
1
28-      26    0                     26                     imp:n,p
0

29-

30-      c Surface
Cards
31-      c solution
cylinder
32-      1     cz    3.0            $ hot H2/LEU cyl
surf
33-      2     cz
3.1
34-      3     cz
3.2
35-      4     cz
3.3
36-      5     cz
3.4
37-      6     cz
3.5
38-      7     cz
3.6
39-      8     cz
3.7
40-      9     cz
3.8
41-      10    cz
3.9
42-      11    cz
4.0
43-      12    cz
4.1
44-      13    cz
4.2
45-      14    cz
4.3
46-      15    cz
4.4
47-      16    cz
4.5
48-      17    cz
4.6
49-      18    cz
```

```
        4.7
        50-       19      cz
        4.8
        51-       20      cz
        4.9
        52-       21      cz      5               $ inner porous centrifuge wall
        surf
        53-       22      cz      6               $ outer porous centrifuge wall
        surf
        54-       23      cz      6.1             $ inner reflect
        surf
        55-       24      cz      7.1             $ outer reflect
        surf
        56-       25      pz      50              $ centrifuge
        top
        57-       c reactor
        vessel
        58-       26      rcc     0 0 -50  0 0 110  50            $ outer Mod
        surf

        59-

        60-       c Data
        Cards
        61-       mode n
        p
  comment.  photonuclear physics may be needed (phys:p).
        62-       kcode   5000 1 20 100   $  Calculate
        keff
        63-       ksrc    0 4.05
        0
        64-       c
        Materials
        65-       M1      1001.84c        1.0             $ Hot H2 @
        2700K
        66-       M2      92235.84c       -0.1975         $ LEU w%U-235
        19.75
        67-               92238.84c
        -0.8025
        68-       M3      3007.86c        -0.97988        $
        Li7H
        69-               1001.86c
        -0.02012
        70-       M4      4009.80c        1.0             $
        Beryllium
        71-       MT4
        be.20t
        72-       M5      6000.82c        -0.995041       $ porous(50%) graphite
        saturated with H2
        73-               1001.82c
        -0.004959
        74-       M6      1002.85c        1.0             $ liquid
        H2
        75-       M7      6000.86c        1.0             $
        graphite
  warning.  material        7 is not used in the problem.
        76-       M7T
        grph.20t
  warning.  material        7 is not used in the problem.
        77-       c
        Tallies
        78-       e0:n    0.1 1.0 20.0            $ Default energy bins
        (MeV)
        79-       f2:n,p  26.1 26.2 26.3 T        $ photon & neutron flux through
        surface
        80-       f4:n    1 2 3 4 5 6 7 8 9 10 11 12 13 14 15             $ flux in
        cells
        81-               16 17 18 19 20 21 22 23 24
        25
```

```
        82-       f6:n,p  1 2 3 4 5 6 7 8 9 10 11 12 13 14 15
        16
        83-              17 18 19 20 21 22 23 24 25      $ energy
        deposition

        84-


  comment.  total fission nubar data are being used.

  warning.    1001.82c and   1001.84c are both called for.

  warning.    1001.84c and   1001.86c are both called for.

  warning.    1 of the materials appear at more than one density.
 1cells
               print table 60

                             atom
                             gram
                             neutron    photon     photon wt
              cell      mat   density     density     volume       mass
              pieces importance importance generation

        1       1       1  3.02409E-04 5.06100E-04 3.11018E+03 1.57406E+00
        1  1.0000E+00 1.0000E+00 -1.000E+00
        2       2       2  1.51579E-04 5.97680E-02 1.91637E+02 1.14538E+01
        1  1.0000E+00 1.0000E+00 -1.000E+00
        3       3       2  1.51703E-04 5.98170E-02 1.97920E+02 1.18390E+01
        1  1.0000E+00 1.0000E+00 -1.000E+00
        4       4       2  1.51845E-04 5.98730E-02 2.04204E+02 1.22263E+01
        1  1.0000E+00 1.0000E+00 -1.000E+00
        5       5       2  6.85888E-03 2.70447E+00 2.10487E+02 5.69256E+02
        1  1.0000E+00 1.0000E+00 -1.000E+00
        6       6       2  3.34893E-02 1.32049E+01 2.16770E+02 2.86243E+03
        1  1.0000E+00 1.0000E+00 -1.000E+00
        7       7       2  3.44551E-02 1.35858E+01 2.23053E+02 3.03034E+03
        1  1.0000E+00 1.0000E+00 -1.000E+00
        8       8       2  3.53941E-02 1.39560E+01 2.29336E+02 3.20062E+03
        1  1.0000E+00 1.0000E+00 -1.000E+00
        9       9       2  3.63078E-02 1.43163E+01 2.35619E+02 3.37319E+03
        1  1.0000E+00 1.0000E+00 -1.000E+00
       10      10       2  3.71973E-02 1.46670E+01 2.41903E+02 3.54799E+03
       1  1.0000E+00 1.0000E+00 -1.000E+00
       11      11       2  3.80641E-02 1.50088E+01 2.48186E+02 3.72497E+03
       1  1.0000E+00 1.0000E+00 -1.000E+00
       12      12       2  3.89092E-02 1.53420E+01 2.54469E+02 3.90406E+03
       1  1.0000E+00 1.0000E+00 -1.000E+00
       13      13       2  3.97336E-02 1.56671E+01 2.60752E+02 4.08523E+03
       1  1.0000E+00 1.0000E+00 -1.000E+00
       14      14       2  4.05385E-02 1.59844E+01 2.67035E+02 4.26841E+03
       1  1.0000E+00 1.0000E+00 -1.000E+00
       15      15       2  4.13246E-02 1.62944E+01 2.73319E+02 4.45356E+03
       1  1.0000E+00 1.0000E+00 -1.000E+00
       16      16       2  4.20928E-02 1.65973E+01 2.79602E+02 4.64064E+03
       1  1.0000E+00 1.0000E+00 -1.000E+00
       17      17       2  4.28440E-02 1.68935E+01 2.85885E+02 4.82960E+03
       1  1.0000E+00 1.0000E+00 -1.000E+00
       18      18       2  4.44166E-02 1.75136E+01 2.92168E+02 5.11691E+03
       1  1.0000E+00 1.0000E+00 -1.000E+00
       19      19       2  4.84399E-02 1.91000E+01 2.98451E+02 5.70042E+03
       1  1.0000E+00 1.0000E+00 -1.000E+00
       20      20       2  4.84399E-02 1.91000E+01 3.04734E+02 5.82043E+03
       1  1.0000E+00 1.0000E+00 -1.000E+00
       21      21       2  4.84399E-02 1.91000E+01 3.11018E+02 5.94044E+03
       1  1.0000E+00 1.0000E+00 -1.000E+00
       22      22       5  4.51482E-02 8.54236E-01 3.45575E+03 2.95203E+03
       1  1.0000E+00 1.0000E+00 -1.000E+00
       23      23       6  2.53305E-03 8.47190E-03 3.80133E+02 3.22045E+00
```

```
comment.
comment. Source entropy convergence check passed.
comment.
the results of the w test for normality applied to the individual collision, absorption, and track-length keff cycle values are:

          the k( collision) cycle values appear normally distributed at the 95 percent confidence level
          the k(absorption) cycle values appear normally distributed at the 95 percent confidence level
          the k(trk length) cycle values appear normally distributed at the 95 percent confidence level



------------------------------------------------------------------------------------------------------------------------------------
|                                                                                                                                  |
| the final estimated combined collision/absorption/track-length keff = 0.88394 with an estimated standard deviation of 0.00121   |
|                                                                                                                                  |
| the estimated 68, 95, & 99 percent keff confidence intervals are 0.88273 to 0.88516, 0.88153 to 0.88636, and 0.88074 to 0.88714 |
|                                                                                                                                  |
| the final combined (col/abs/tl) prompt removal lifetime = 7.6118E-04 seconds with an estimated standard deviation of 1.3717E-05 |
|                                                                                                                                  |
| the average neutron energy causing fission = 4.0417E-01 mev                                                                     |
| the energy corresponding to the average neutron lethargy causing fission = 1.9465E-05 mev                                       |
|                                                                                                                                  |
| the percentages of fissions caused by neutrons in the thermal, intermediate, and fast neutron ranges are:                       |
|         (<0.625 ev):  50.18%         (0.625 ev - 100 kev):  28.88%          (>100 kev):  20.94%                                 |
|                                                                                                                                  |
| the average fission neutrons produced per neutron absorbed (capture + fission) in all cells with fission = 1.7519E+00           |
| the average fission neutrons produced per neutron absorbed (capture + fission) in all the geometry cells = 1.1759E+00           |
|                                                                                                                                  |
| the average number of neutrons produced per fission = 2.481                                                                     |
|                                                                                                                                  |
------------------------------------------------------------------------------------------------------------------------------------


the estimated average keffs, one standard deviations, and 68, 95, and 99 percent confidence intervals are:

```

```
the first active half of the problem skips 20 cycles and uses  40 active cycles; the
second half skips  60 and uses  40 cycles.
the col/abs/trk-len keff, one standard deviation, and 68, 95, and 99 percent intervals
for each active half of the problem are:

             problem        keff     standard deviation       68% confidence
             95% confidence         99% confidence

           first half     0.88310         0.00172           0.88136 to 0.88484
           0.87961 to 0.88659     0.87842 to 0.88778
          second half     0.88484         0.00177           0.88306 to 0.88663
          0.88126 to 0.88842     0.88005 to 0.88964
         final result     0.88394         0.00121           0.88273 to 0.88516
         0.88153 to 0.88636     0.88074 to 0.88714

the first and second half values of k(collision/absorption/track length) appear to be
the same at the 68 percent confidence level.

1tally        4        nps =      499664
          tally type 4    track length estimate of particle flux.      units
          1/cm**2
          particle(s): neutrons
number of histories used for normalizing tallies =       400000.00

          volumes
                  cell:       1           2           3           4
                  5           6           7
                        3.11018E+03  1.91637E+02  1.97920E+02  2.04204E+02
                        2.10487E+02  2.16770E+02  2.23053E+02
                  cell:       8           9          10          11
                  12          13          14
                        2.29336E+02  2.35619E+02  2.41903E+02  2.48186E+02
                        2.54469E+02  2.60752E+02  2.67035E+02
                  cell:      15          16          17          18
                  19          20          21
                        2.73319E+02  2.79602E+02  2.85885E+02  2.92168E+02
                        2.98451E+02  3.04734E+02  3.11018E+02
                  cell:      22          23          24
                  25
                        3.45575E+03  3.80133E+02  4.14690E+03  8.47818E+05

cell
1

     energy
   1.0000E-01   3.91664E-04 0.0042
   1.0000E+00   5.52768E-04 0.0036
   2.0000E+01   3.66582E-04 0.0041
     total      1.31101E-03 0.0023

cell
2

     energy
   1.0000E-01   3.98594E-04 0.0048
   1.0000E+00   6.14332E-04 0.0041
   2.0000E+01   4.13450E-04 0.0047
     total      1.42638E-03 0.0026

cell
3

     energy
   1.0000E-01   3.95625E-04 0.0048
   1.0000E+00   6.15733E-04 0.0040
   2.0000E+01   4.17378E-04 0.0047
     total      1.42874E-03 0.0025
```

```
3.16+01     27 1.04-05  -4.984 *****************|***             |        s
|               |                |
3.98+01      6 1.83-06  -5.737 ********         |                |     s
|               |                |
5.01+01      6 1.46-06  -5.837 ******           |                | s
|               |                |
6.31+01     12 2.31-06  -5.636 **********       |               s|
|               |                |
7.94+01      5 7.65-07  -6.116 *                |           s    |
|               |                |
1.00+02      6 7.29-07  -6.137 *                |       s        |
|               |                |
 total  159503 3.99-01
 d----------------d----------------d-----------------d-----------------d----------------
 -d-----------

1tally        6        nps =      499664
           tally type 6    track length estimate of heating.            units
           mev/gram
           particle(s): neutrons  photons
 number of histories used for normalizing tallies =       400000.00

           masses
                   cell:       1           2           3           4
                   5           6           7
                         1.57406E+00  1.14538E+01  1.18390E+01  1.22263E+01
                         5.69256E+02  2.86243E+03  3.03034E+03
                   cell:       8           9          10          11
                   12          13          14
                         3.20062E+03  3.37319E+03  3.54799E+03  3.72497E+03
                         3.90406E+03  4.08523E+03  4.26841E+03
                   cell:      15          16          17          18
                   19          20          21
                         4.45356E+03  4.64064E+03  4.82960E+03  5.11691E+03
                         5.70042E+03  5.82043E+03  5.94044E+03
                   cell:      22          23          24
                   25
                         2.95203E+03  3.22045E+00  3.24702E+03  1.56846E+06

 cell
 1

      energy
    1.0000E-01   4.34177E-05 0.0063
    1.0000E+00   4.60398E-04 0.0036
    2.0000E+01   6.74903E-04 0.0041
      total      1.17872E-03 0.0027

 cell
 2

      energy
    1.0000E-01   2.66051E-04 0.0144
    1.0000E+00   7.76408E-05 0.0038
    2.0000E+01   1.15375E-04 0.0045
      total      4.59067E-04 0.0085

 cell
 3

      energy
    1.0000E-01   2.61474E-04 0.0129
    1.0000E+00   7.77843E-05 0.0038
    2.0000E+01   1.16213E-04 0.0045
      total      4.55472E-04 0.0075

 cell
 4
```

```
      energy
    1.0000E-01   2.55082E-04 0.0113
    1.0000E+00   7.82706E-05 0.0038
    2.0000E+01   1.17579E-04 0.0044
      total      4.50931E-04 0.0066

cell
5

      energy
    1.0000E-01   2.44964E-04 0.0095
    1.0000E+00   7.87479E-05 0.0037
    2.0000E+01   1.17989E-04 0.0043
      total      4.41700E-04 0.0055

cell
6

      energy
    1.0000E-01   2.33354E-04 0.0077
    1.0000E+00   7.91752E-05 0.0034
    2.0000E+01   1.18645E-04 0.0040
      total      4.31174E-04 0.0044

cell
7

      energy
    1.0000E-01   2.25796E-04 0.0069
    1.0000E+00   7.97257E-05 0.0033
    2.0000E+01   1.20013E-04 0.0039
      total      4.25534E-04 0.0039

cell
8

      energy
    1.0000E-01   2.23873E-04 0.0064
    1.0000E+00   7.99264E-05 0.0032
    2.0000E+01   1.21318E-04 0.0037
      total      4.25117E-04 0.0036

cell
9

      energy
    1.0000E-01   2.26951E-04 0.0062
    1.0000E+00   8.02480E-05 0.0031
    2.0000E+01   1.22145E-04 0.0036
      total      4.29344E-04 0.0036

cell
10

      energy
    1.0000E-01   2.31420E-04 0.0061
    1.0000E+00   8.06878E-05 0.0030
    2.0000E+01   1.22493E-04 0.0035
      total      4.34601E-04 0.0035

cell
11

      energy
    1.0000E-01   2.40245E-04 0.0060
    1.0000E+00   8.09582E-05 0.0030
    2.0000E+01   1.24229E-04 0.0034
      total      4.45433E-04 0.0034
```

```
cell
12

    energy
   1.0000E-01   2.53460E-04 0.0058
   1.0000E+00   8.14408E-05 0.0029
   2.0000E+01   1.25999E-04 0.0034
     total      4.60900E-04 0.0034

cell
13

    energy
   1.0000E-01   2.70570E-04 0.0057
   1.0000E+00   8.18886E-05 0.0028
   2.0000E+01   1.27269E-04 0.0033
     total      4.79727E-04 0.0034

cell
14

    energy
   1.0000E-01   2.95127E-04 0.0057
   1.0000E+00   8.22675E-05 0.0028
   2.0000E+01   1.29374E-04 0.0033
     total      5.06768E-04 0.0035

cell
15

    energy
   1.0000E-01   3.30298E-04 0.0056
   1.0000E+00   8.28928E-05 0.0027
   2.0000E+01   1.31225E-04 0.0032
     total      5.44416E-04 0.0035

cell
16

    energy
   1.0000E-01   3.80192E-04 0.0055
   1.0000E+00   8.36352E-05 0.0026
   2.0000E+01   1.33559E-04 0.0031
     total      5.97387E-04 0.0036

cell
17

    energy
   1.0000E-01   4.59363E-04 0.0053
   1.0000E+00   8.45924E-05 0.0026
   2.0000E+01   1.36398E-04 0.0031
     total      6.80353E-04 0.0037

cell
18

    energy
   1.0000E-01   5.94594E-04 0.0050
   1.0000E+00   8.57502E-05 0.0025
   2.0000E+01   1.40085E-04 0.0030
     total      8.20429E-04 0.0037

cell
19

    energy
   1.0000E-01   8.50686E-04 0.0045
   1.0000E+00   8.75293E-05 0.0025
```

```
    2.0000E+01   1.44803E-04 0.0030
      total      1.08302E-03 0.0036

cell
20

      energy
    1.0000E-01   1.40953E-03 0.0038
    1.0000E+00   8.98949E-05 0.0024
    2.0000E+01   1.49875E-04 0.0029
      total      1.64930E-03 0.0033

cell
21

      energy
    1.0000E-01   3.08790E-03 0.0030
    1.0000E+00   9.25687E-05 0.0023
    2.0000E+01   1.50971E-04 0.0027
      total      3.33144E-03 0.0028

cell
22

      energy
    1.0000E-01   7.49227E-07 0.0037
    1.0000E+00   1.14453E-05 0.0024
    2.0000E+01   2.36452E-05 0.0026
      total      3.58397E-05 0.0019

cell
23

      energy
    1.0000E-01   4.74226E-06 0.0046
    1.0000E+00   9.68406E-05 0.0029
    2.0000E+01   2.14180E-04 0.0028
      total      3.15763E-04 0.0020

cell
24

      energy
    1.0000E-01   1.24860E-06 0.0032
    1.0000E+00   1.56405E-05 0.0021
    2.0000E+01   3.35636E-05 0.0023
      total      5.04527E-05 0.0016

cell
25

      energy
    1.0000E-01   8.38639E-08 0.0015
    1.0000E+00   5.70470E-07 0.0017
    2.0000E+01   1.23694E-06 0.0026
      total      1.89127E-06 0.0019


***** the nps-dependent tfc bin check results are suspect because there are only  1
nps tally values to analyze *****



==========================================================================================
============================================

          results of 10 statistical checks for the estimated answer for the tally
          fluctuation chart (tfc) bin of tally        6

```

```
tfc bin     --mean--      ---------relative error---------      ----variance of the
variance----      --figure of merit--     -pdf-
behavior    behavior      value   decrease   decrease rate      value   decrease
decrease rate       value     behavior     slope

desired      random       <0.10      yes      1/sqrt(nps)       <0.10      yes
1/nps           constant    random      >3.00
observed     random        0.00      yes          yes            0.00      yes
yes            constant    random       9.76
passed?        yes          yes      yes          yes             yes      yes
yes               yes        yes         yes


==========================================================================================
===========================================



this tally meets the statistical criteria used to form confidence intervals: check the
tally fluctuation chart to verify.
the results in other bins associated with this tally may not meet these statistical
criteria.

----- estimated confidence intervals:  -----

estimated asymmetric confidence interval(1,2,3 sigma): 1.1756E-03 to 1.1819E-03;
1.1724E-03 to 1.1851E-03; 1.1692E-03 to 1.1882E-03
estimated  symmetric confidence interval(1,2,3 sigma): 1.1756E-03 to 1.1819E-03;
1.1724E-03 to 1.1850E-03; 1.1692E-03 to 1.1882E-03

1analysis of the results in the tally fluctuation chart bin (tfc) for tally       6
with nps =      499664  print table 160


 normed average tally per history  = 1.17872E-03          unnormed average tally per
 history  = 1.85537E-03
 estimated tally relative error    = 0.0027               estimated variance of the
 variance  = 0.0001
 relative error from zero tallies  = 0.0015               relative error from nonzero
 scores  = 0.0022

 number of nonzero history tallies =      211767          efficiency for the nonzero
 tallies  = 0.5294
 history number of largest  tally  =      108618          largest  unnormalized history
 tally = 8.74292E-02
 (largest  tally)/(average tally)  = 4.71222E+01          (largest  tally)/(avg nonzero
 tally)= 2.49473E+01

 (confidence interval shift)/mean  = 0.0000               shifted confidence interval
 center  = 1.17873E-03


 if the largest  history score sampled so far were to occur on the next history, the
 tfc bin quantities would change as follows:
 nps =      400513 for this table because  20 keff cycles and       99151 histories
 were skipped before tally accumulation.

      estimated quantities           value at nps           value at nps+1
      value(nps+1)/value(nps)-1.

      mean                            1.17872E-03
      1.17885E-03                     0.000115
      relative error                  2.68439E-03
      2.68714E-03                     0.001026
      variance of the variance        5.83958E-05
      6.15324E-05                     0.053712
      shifted center                  1.17873E-03
      1.17873E-03                     0.000000
      figure of merit                 5.24856E+04
      5.23781E+04                    -0.002049
```

```
 the estimated inverse power slope of the 198 largest  tallies starting at 3.00801E-02
 is 9.7646
 the large score tail of the empirical history score probability density function
 appears to have no unsampled regions.

 fom = (histories/minute)*(f(x) signal-to-noise ratio)**2 = (1.513E+05)*( 5.890E-01)**2
 = (1.513E+05)*(3.469E-01) = 5.249E+04

1status of the statistical checks used to form confidence intervals for the mean for
each tally bin


 tally   result of statistical checks for the tfc bin (the first check not passed is
 listed) and error magnitude check for all bins

        4   passed the 10 statistical checks for the tally fluctuation chart bin
        result
         passed all bin error check:   100 tally bins all have relative errors less
         than 0.10 with no zero bins

        2   missed  1 of 10 tfc bin checks: the slope of decrease of largest tallies is
        less than the minimum acceptable value of 3.0
         passed all bin error check:    16 tally bins all have relative errors less
         than 0.10 with no zero bins

        6   passed the 10 statistical checks for the tally fluctuation chart bin
        result
         passed all bin error check:   100 tally bins all have relative errors less
         than 0.10 with no zero bins


 the 10 statistical checks are only for the tally fluctuation chart bin and do not
 apply to other tally bins.

 warning.       1 of the     3 tally fluctuation chart bins did not pass all 10
 statistical checks.
1tally fluctuation charts

                             tally        4                          tally
                             2                           tally        6
          nps      mean     error   vov  slope    fom      mean     error   vov
          slope    fom      mean     error   vov  slope    fom
       499664   1.3110E-03 0.0023 0.0000 10.0   74463   1.9290E-05 0.0035 0.0010  1.9
       30115   1.1787E-03 0.0027 0.0001  9.8   52486


 ****************************************************************************************
 *******************************

 dump no.    2 on file INP_U_OD_10_ID_6_dens_prof_pure_vls_4r     nps =      499664
 coll =      135022750     ctm =
       3.09   nrn =       1253109253

        11 warning messages so far.


 run terminated when     100 kcode cycles were done.

 computer time =    3.11 minutes

 mcnp     version 6     05/08/13                    04/27/20
 10:03:46                    probid =  04/27/20 10:00:27
```